

# Distributed Control for a Robotic Swarm to Pass through a Curve Virtual Tube

Journal Title  
 XX(X):1–18  
 ©The Author(s) 2021  
 Reprints and permission:  
 sagepub.co.uk/journalsPermissions.nav  
 DOI: 10.1177/ToBeAssigned  
 www.sagepub.com/

SAGE

Quan Quan, Yan Gao, Chenggang Bai

## Abstract

Robotic swarm systems are now becoming increasingly attractive for many challenging applications. The main task for any robot is to reach the destination while keeping a safe separation from other robots and obstacles. In many scenarios, robots need to move within a narrow corridor, through a window or a doorframe. In order to guide all robots to move in a cluttered environment, a curve virtual tube with no obstacle inside is carefully designed in this paper. There is no obstacle inside the tube, namely the area inside the tube can be seen as a safety zone. Then, a distributed swarm controller is proposed with three elaborate control terms: a line approaching term, a robot avoidance term and a tube keeping term. Formal analysis and proofs are made to show that the curve virtual tube passing problem can be solved in a finite time. For the convenience in practical use, a modified controller with an approximate control performance is put forward. Finally, the effectiveness of the proposed method is validated by numerical simulations and real experiments. To show the advantages of the proposed method, the comparison between our method and the control barrier function method is also presented in terms of calculation speed.

## Keywords

Distributed control, swarm, vector field, artificial potential field, virtual tube

## 1 Introduction

Recently, advances in research have brought robotic swarm systems to a level of sophistication which makes it increasingly attractive for a variety of complex applications like sensing, mapping, search and rescue Chung et al. (2018). In order to make these applications a reality, it is necessary for the robotic swarm to have the ability to operate in a cluttered environment and reach the appointed destination in a distributed way. Moving within a narrow corridor, through a window or a doorframe is a very common scenario Turpin et al. (2014). In this process, not only should each robot avoid collisions with obstacles, but all robots also need to avoid collisions with each other.

Many successful methods have been put forward for planning and controlling multiple robots in a cluttered environment. The typical methods can mainly be classified into three types: formation, multi-agent trajectory planning and control-based methods. The *formation* here refers specifically to all robots keeping a geometry structure as a whole, which suits both semi-autonomous and fully-autonomous control Ren and Sorensen (2008), Cheung et al. (2009), Chen et al. (2010), Oh et al. (2015), Khan et al. (2016), Zhao and Zelazo (2019), Saska et al. (2020), Dong and Sitti (2020). Each robot in the formation usually remains a prespecified pose and makes the formation stable and robust. The pilot or the control program can control the formation to avoid the obstacles in the environment, which is like controlling a single robot. The inter-robot collision avoidance is mainly achieved by the fixed geometry. When the formation operates in a cluttered environment and needs to pass through some narrow spaces or corridors, necessary transformations have to be carried out Zhao

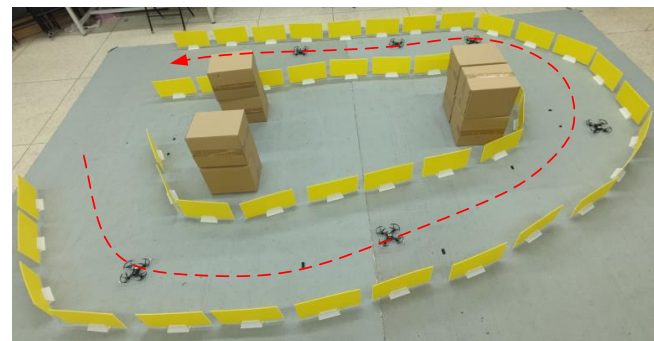


**Figure 1.** A curve virtual tube is designed for guiding a multicopter swarm in a cluttered environment.

and Zelazo (2019). The affine formation maneuver control is especially suitable for the transformation control Xu et al. (2020). However, the formation is not perfect in all circumstances and the main weakness is its limited scalability and adaptability. If there are hundreds or even thousands of robots, the increase in quantity leads to the expansion of the physical size and the formation will be too big to maintain feasibility Hao et al. (2016). Besides, when some robots need to change their locations, it may cause

School of Automation Science and Electrical Engineering, Beihang University, Beijing 100191, P. R. China

### Corresponding author:

Quan Quan, School of Automation Science and Electrical Engineering, Beihang University, Beijing 100191, P. R. China.  
 Email: qq\_buaa@buaa.edu.cn

chaos in the formation and the controller will become very complex.

The *multi-agent trajectory planning* produces collision-free trajectories with higher-order continuity for all robots in a centralized or distributed way Mellinger et al. (2012), Augugliaro et al. (2012), Turpin et al. (2014), Luo et al. (2019), Morgan et al. (2016), Tang et al. (2018), Luis and Schoellig (2019), Park et al. (2020), Zhou et al. (2021). Different from the velocity or acceleration command of the formation control, the higher-order trajectory, such as Bezier curves Park et al. (2020) and B-splines Zhou et al. (2021), can get a better control performance especially for the multicopter. Given a specific target point, any robot should find a discrete geometric path in the global map first and then optimize the path to a feasible trajectory locally with no conflict with obstacles and other robots' trajectories Ding et al. (2019). However, when there are multiple robots operating densely, trajectories planning becomes inappropriate intuitively and infeasible in real practice, the reason of which is the sharp increase in computational complexity and decrease of the feasible region Augugliaro et al. (2012), Chen et al. (2016). Besides, distributed multi-agent trajectory planning needs any robot to share its planned trajectory with others via wireless communication, which brings a huge communication pressure when the number of robots increases Zhou et al. (2021). The communication uncertainties, such as broadcast delay and packet loss, can also make the trajectory optimization infeasible under some circumstances Tahir et al. (2019).

For robotic *swarm* navigation and control, the control-based methods are widely used because of their simplicity and accessibility Wolf and Burdick (2008). Control-based methods usually use a simple controller to react to obstacles or other robots, which have a good quality to achieve a fast and reactive response to a dynamic environment and a low demand for computation and communication resources. Different from the multi-agent trajectory planning, the *control-based methods* directly guide the robots' movement with the velocity or acceleration command according to the global path and current local information Miao et al. (2016), Wang et al. (2017), Quan et al. (2021b). Although the control-based methods possess a weaker control performance compared with the multi-robot trajectory planning Luis and Schoellig (2019), Park et al. (2020), Zhou et al. (2021), they are more suitable for the large-scale robotic swarm, such as the potential-based method Quan et al. (2021b) and the vector field method Miao et al. (2016), which directly guide the robots' movement according to the global path and current local information Wang et al. (2017). Besides, the control barrier function (CBF) method is also popular in recent years, which is summarized as a quadratic programming (QP) problem with better performance and higher demand on the computational resources Wang et al. (2017).

The method proposed in this paper is a modified type of the artificial potential field (APF) method belonging to the control-based method. The APF method was first introduced for manipulator control by Khatib Khatib (1986), which can be also seen as a gradient vector field method. In contrast, there are also non-potential vector field methods with curls non-zero Panagou (2014), Panagou (2016). Compared with

the CBF method, the APF method is especially suitable for dealing with multi-objective compositions at the same time. The task of the multi-objective composition is rather complicated for the CBF method, as multiple hard safety constraints may cause no feasible solution. Existing literature is limited to the combination of similar and complementary objectives, such as collision avoidance and connectivity maintenance Wang et al. (2016). For the APF method, each control objective can be described as a potential function, either attractive or repulsive. By summing up all potential functions, the corresponding vector field is directly generated with a gradient operation. Nevertheless, inappropriate definitions of the potential field will cause various problems, in which the most serious is local minima Hernández-Martínez and Aranda-Bricaire (2011). The local minima problem is the appearance of unexpected equilibrium points where the composite potential field vanishes. This problem has limited the extensive application of the APF method. In the literature, there exist many different approaches to deal with the local minima problem while ensuring convergence and safety. Some approaches are willing to keep the robots away from or make robots leave from these deadlock points. In Rostami et al. (2019), the local minima are avoided by orthogonal decomposition of the repulsive component in the direction of parallel and perpendicular to the attractive component. In Antich and Ortiz (2005), Ge and Fua (2005), small disturbances are imposed to make robots escape local minima. Another kind of solution is to improve the APF method with optimization approaches, such as the evolutionary artificial potential field method Vadakkepat et al. (2000), in which the APF method is combined with genetic algorithms to derive optimal potential field functions. Besides, in Kim and Khosla (1992), the harmonic potential functions are introduced, whose undesired equilibrium points are all saddle points. The Morse function has a similar property, that is, all undesired local minima disappears as  $\delta$  increases Rimon (1990), Panagou et al. (2015).

Motivated by the current studies, a *curve virtual tube* is presented for guiding the robotic swarm in a cluttered environment. The term “virtual tube” appears in the AIRBUS’s Skyways project, which enables unmanned airplanes to fly over the cities Airbus (2019). In our previous work Quan et al. (2021b), the *straight-line virtual tube* is proposed for the air traffic control as flight routes are usually composed of several line segments. There is no obstacle inside the virtual tube and the area inside can be taken as a safety zone. In other words, the robots in the virtual tube have no need to consider conflicts with obstacles and only need to guarantee no collision with each other and the tube boundary. In this paper, the concept of the virtual tube is generalized. Compared with the straight-line virtual tube, the proposed curve virtual tube is generated along a continuous generating curve and the radius or width of the virtual tube is mutable. Hence, the curve virtual tube is more suitable for guiding the robotic swarm to move within a narrow corridor, through a window or a doorframe. Some similar concepts have been proposed in the literature. As shown in Fig. 1, the concept of the curve virtual tube is similar to the lane for autonomous road vehicles in Rasekhipour

et al. (2016), Luo et al. (2018) and the corridor for a multi-UAV system in Tony et al. (2020). In Rasekhipour et al. (2016), autonomous road vehicles are restricted to moving inside the lane with a potential-field-based model predictive path planning controller. In Liu et al. (2017), a trajectory generation method using a safe flight corridor is proposed for a single multicopter, which defines a piecewise Bezier curve within the corridor by utilizing the convex hull property. In Tony et al. (2020), the authors proposed a multi-drone skyway framework called CORRIDRONE, which is one such architecture that generates corridors for point-to-point traversal of several drones.

For controlling the robotic swarm with our proposed curve virtual tube, two problems are summarized, namely *curve virtual tube planning problem* and *curve virtual tube passing problem*. This paper only aims to solve the latter one. For the curve virtual tube planning problem, the generating curve can be automatically obtained by interpolating with several waypoints, which can be generated from the traditional sampling-based Likhachev et al. (2003), Dolgov et al. (2010), Harabor and Grastien (2011), Gammell et al. (2014), Gammell et al. (2015), or search-based methods Kavraki et al. (1996), LaValle and Kuffner Jr (2001). Another feasible approach is to utilize an existing trajectory as the generating curve, which performs like a “teach-and-repeat” system Gao et al. (2019). Then the curve virtual tube is generated by expanding the generating curve and there must be no conflict with obstacles. The curve virtual tube passing problem is solved in this paper with a distributed gradient vector field method. It should be noted that there is no uncertainty considered in this paper, namely all robots are able to obtain the information clearly and execute the velocity command exactly. For the real practice with various uncertainties, the *separation theorem* can be introduced, which is proposed in our previous work Quan et al. (2021a), to solve the uncertainty problem. In short, all uncertainties are considered in the design of the safety radius of the robot, which is beyond the scope of this paper. Here, two models for robots and the curve virtual tube are first proposed. The robot model is a single integral model and the curve virtual tube model is set up with the concept of the generating curve and the cross section. To ensure all robots can reach the finishing line, a novel *Line-integral Lyapunov function* is proposed. Then, the single panel method and a Lyapunov-like barrier function are proposed for restricting robots to moving inside the curve virtual tube and avoiding collision with each other. Based on these functions and methods, a distributed swarm controller with a saturation constraint is designed. For practical use, a modified swarm controller with a similar control effect is also presented. It is proved that all robots are able to pass through the curve virtual tube and there is no local minima with *invariant set theorem* (Slotine et al. 1991, p. 69).

The major contributions of this paper are summarized as follows.

- (i) Based on the straight-line virtual tube introduced in our previous work Quan et al. (2021b), the curve virtual tube is proposed along with some concepts strictly defined with proper mathematical forms. The curve virtual tube is especially suitable for guiding the robotic swarm (tens of thousands of robots) to

move within a narrow corridor, through a window or doorframe. This work makes a significant advance over existing planning and formation methods. Also, this work opens a new way of planning from “one-robot, one-dimensional curve” to “swarm-robot, two (three)-dimensional tube”.

- (ii) A distributed swarm controller is proposed for the curve virtual tube passing problem. Compared with the straight-line virtual tube passing problem introduced in Quan et al. (2021b), the curve virtual tube passing problem in this paper is more complicated and more general. With some active detection devices, such as cameras or radars, the proposed controller can work autonomously without wireless communication and other robots’ IDs. The proposed controller is also very simple and can be computed at a high frequency, which is more suitable for the commonly used single-chip microcomputer. The calculation time of finding feasible solutions for our method and the CBF method is compared in a simulation.
- (iii) A formal proof is proposed to show that there is no collision among robots, and all robots can keep within the tube and pass through the finishing line without getting stuck. The key to the proof is the use of the single panel method, which ensures that the angle between the orientation of the virtual tube keeping term and the orientation of the line approaching term is always smaller than 90°.

The rest of this paper is organized as follows. Section 2 presents two models for the robot and the curve virtual tube. Then the curve virtual tube passing problem is formulated. Section 3 presents some preliminaries. Section 4 provides a distributed controller for the problem. Simulations and experiments are provided for supporting the theoretical results in Section 5 and Section 6, respectively. Finally, Section 7 discusses future work and concludes the paper.

## 2 Problem Formulation

### 2.1 Robot Model

The robotic swarm consists of  $M$  mobile robots in  $\mathbb{R}^2$ . For the vector field design and analysis, each robot has a single integral holonomic kinematics

$$\dot{\mathbf{p}}_i = \mathbf{v}_{c,i}, \quad (1)$$

in which  $\mathbf{v}_{c,i} \in \mathbb{R}^2$ ,  $\mathbf{p}_i \in \mathbb{R}^2$  are the velocity command and position of the  $i$ th robot, respectively. It should be noted that  $\mathbf{v}_{c,i}$  is just the vector field to be designed. In the following,  $\mathbf{v}_{c,i}$  is only called as the *velocity command*. Besides,  $v_{m,i} > 0$  is set as the maximum permitted speed of the  $i$ th robot. Hence it is necessary to make  $\mathbf{v}_{c,i}$  subject to a saturation function

$$\begin{aligned} \mathbf{v}_{c,i} &= \text{sat}(\mathbf{v}'_{c,i}, v_{m,i}) \\ &= \kappa_{v_{m,i}}(\mathbf{v}'_{c,i}) \mathbf{v}'_{c,i}, \end{aligned}$$

where  $\mathbf{v}'_{c,i} \in \mathbb{R}^2$  is the original velocity command and

$$\text{sat}(\mathbf{v}'_{c,i}, v_{m,i}) \triangleq \begin{cases} \mathbf{v}'_{c,i} & \|\mathbf{v}'_{c,i}\| \leq v_{m,i} \\ v_{m,i} \frac{\mathbf{v}'_{c,i}}{\|\mathbf{v}'_{c,i}\|} & \|\mathbf{v}'_{c,i}\| > v_{m,i} \end{cases}$$

$$\kappa_{v_{m,i}}(\mathbf{v}'_{c,i}) \triangleq \begin{cases} 1 & \|\mathbf{v}'_{c,i}\| \leq v_{m,i} \\ \frac{v_{m,i}}{\|\mathbf{v}'_{c,i}\|} & \|\mathbf{v}'_{c,i}\| > v_{m,i} \end{cases}.$$

It is obvious that  $0 < \kappa_{v_{m,i}}(\mathbf{v}'_{c,i}) \leq 1$ . In the following,  $\kappa_{v_{m,i}}(\mathbf{v}'_{c,i})$  will be written as  $\kappa_{v_{m,i}}$  for short. When a given robot is modeled as a single integrator just as (1), such as multicopters, helicopters and certain types of wheeled robots equipped with omni-directional wheels Quan (2017), the designed velocity command  $\mathbf{v}_{c,i}$  can be directly applied to control the robot. When the robot model considered is more complicated, such as a second order integrator model, additional control laws are necessary Rezende et al. (2020). Besides, in our previous work Quan et al. (2021b), we propose a *filtered position model* converting a second-order model to a first-order model just as (1).

## 2.2 Curve Virtual Tube Model

Before the curve virtual tube is introduced, some necessary concepts are first proposed.

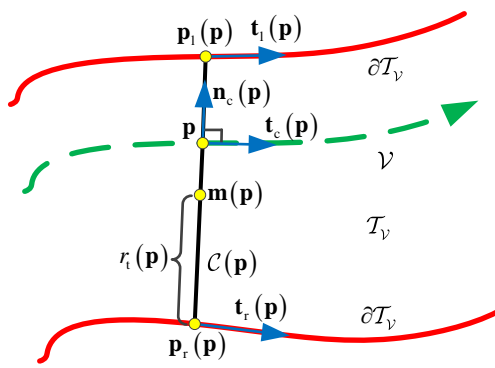


Figure 2. Relative concepts about the curve virtual tube.

(i) **Generating Curve.** A curve in  $\mathbb{R}^2$  is *simple* if it does not cross itself. When a curve starts and ends at the same point, it is a *closed curve* or *loop* (Thomas et al. 2003, p. 915). In this paper, we only consider a simple and not closed *generating curve*  $\mathcal{V} \subset \mathbb{R}^2$ , which starts at  $\mathbf{p}_s \in \mathcal{V}$  and ends at  $\mathbf{p}_f \in \mathcal{V}$ . As shown in Figure 2, if there exists  $\mathbf{p} \in \mathcal{V}$ , define  $\mathbf{t}_c(\mathbf{p}) \in \mathbb{R}^2$  to be the *unit tangent vector* pointing in the forward direction, namely the moving direction. Similarly,  $\mathbf{n}_c(\mathbf{p}) \in \mathbb{R}^2$  is the *unit normal vector* directing anti-clockwise or left of the tangent direction. Then it is obtained that

$$\mathbf{t}_c^T(\mathbf{p}) \mathbf{n}_c(\mathbf{p}) \equiv 0.$$

In the following, the generating curve  $\mathcal{V}$  is considered as predefined by planning, namely this paper does not cover how to design  $\mathcal{V}$ .

(ii) **Cross Section.** For any  $\mathbf{p} \in \mathcal{V}$ , a *cross section* passing  $\mathbf{p}$  is defined as

$$\mathcal{C}(\mathbf{p}) = \{ \mathbf{x} \in \mathbb{R}^2 : \mathbf{x} = \mathbf{p} + \lambda(\mathbf{p}) \mathbf{n}_c(\mathbf{p}), \lambda_l(\mathbf{p}) \leq \lambda(\mathbf{p}) \leq \lambda_r(\mathbf{p}), \lambda_l(\mathbf{p}), \lambda_r(\mathbf{p}) \in \mathbb{R} \}.$$

Here,  $\mathcal{C}(\mathbf{p}_f)$  is called the *finishing line* or *finishing cross section*. For any point  $\mathbf{p}' \in \mathcal{C}(\mathbf{p})$ ,  $\mathcal{C}(\mathbf{p}')$  is defined as a cross section passing  $\mathbf{p}'$ . It is obvious that

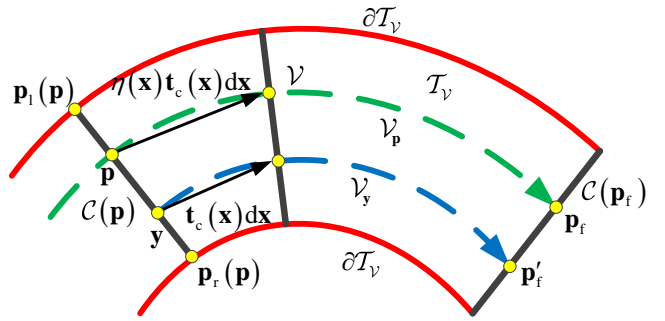


Figure 3. Brief introduction to the length and the equation (7).

$\mathcal{C}(\mathbf{p}') = \mathcal{C}(\mathbf{p})$ . Besides, it has  $\mathbf{t}_c(\mathbf{p}') = \mathbf{t}_c(\mathbf{p})$ . For  $\mathbf{x}_1 \in \mathcal{C}(\mathbf{p}_1)$ ,  $\mathbf{x}_2 \in \mathcal{C}(\mathbf{p}_2)$  and  $\mathbf{p}_1, \mathbf{p}_2 \in \mathcal{V}$ , if a point can move along the tangent vector  $\mathbf{t}_c(\cdot)$  from  $\mathbf{p}_1$  to  $\mathbf{p}_2$ , then we say  $\mathbf{x}_1$  or  $\mathcal{C}(\mathbf{p}_1)$  locates at *back* of  $\mathcal{C}(\mathbf{p}_2)$ . In other words,  $\mathbf{x}_2$  or  $\mathcal{C}(\mathbf{p}_2)$  locates at *front* of  $\mathcal{C}(\mathbf{p}_1)$ . Two endpoints of  $\mathcal{C}(\mathbf{p})$  are defined as

$$\begin{aligned} \mathbf{p}_l(\mathbf{p}) &\triangleq \mathbf{p} + \lambda_l(\mathbf{p}) \mathbf{n}_c(\mathbf{p}), \\ \mathbf{p}_r(\mathbf{p}) &\triangleq \mathbf{p} + \lambda_r(\mathbf{p}) \mathbf{n}_c(\mathbf{p}). \end{aligned}$$

The *width* of a cross section  $\mathcal{C}(\mathbf{p})$  is expressed as  $2r_t(\mathbf{p})$ , which is defined as

$$r_t(\mathbf{p}) \triangleq \frac{1}{2} |\lambda_r(\mathbf{p}) - \lambda_l(\mathbf{p})|.$$

For any  $\mathbf{p}' \in \mathcal{C}(\mathbf{p})$ , the *middle point* of  $\mathcal{C}(\mathbf{p})$  is defined as

$$\mathbf{m}(\mathbf{p}') = \mathbf{m}(\mathbf{p}) \triangleq \frac{1}{2} (\mathbf{p}_l(\mathbf{p}) + \mathbf{p}_r(\mathbf{p})).$$

Based on the concepts of the generating curve and the cross section, a curve virtual tube model is proposed. The length of the curve virtual tube is also defined.

(i) **Curve Virtual Tube.** The curve virtual tube  $\mathcal{T}_V$  is generated by keeping cross sections always perpendicular to the tangent vectors of the given generating curve, which is denoted by

$$\mathcal{T}_V = \bigcup_{\mathbf{p} \in \mathcal{V}} \mathcal{C}(\mathbf{p}). \quad (2)$$

Then the *tube boundary*  $\partial\mathcal{T}_V$  is expressed as

$$\partial\mathcal{T}_V = \{ \mathbf{x} \in \mathbb{R}^2 : \mathbf{x} = \mathbf{p}_l(\mathbf{p}) \cup \mathbf{p}_r(\mathbf{p}), \mathbf{p} \in \mathcal{V} \}.$$

It is obvious that  $\partial\mathcal{T}_V$  corresponds to two smooth boundary curves as shown in Figure 2. Similar with  $\mathbf{t}_c(\mathbf{p})$ , the vectors  $\mathbf{t}_l(\mathbf{p})$  and  $\mathbf{t}_r(\mathbf{p})$  are defined to be the unit tangent vectors of two tube boundary curves. Besides, for any point  $\mathbf{p}' \in \mathcal{C}(\mathbf{p})$ , it has  $\mathbf{t}_l(\mathbf{p}') = \mathbf{t}_l(\mathbf{p})$  and  $\mathbf{t}_r(\mathbf{p}') = \mathbf{t}_r(\mathbf{p})$ .

(ii) **Length.** As shown in Figure 3, given a point  $\mathbf{y} \in \mathcal{C}(\mathbf{p})$ ,  $\mathcal{V}_y$  is defined to be the curve from  $\mathbf{y}$  to  $\mathcal{C}(\mathbf{p}_f)$  along the tangent vector  $\mathbf{t}_c(\cdot) \in \mathbb{R}^2$ , namely the arc from  $\mathbf{y}$  to  $\mathbf{p}'_f \in \mathcal{C}(\mathbf{p}_f)$ . It can be seen that the curve  $\mathcal{V}_y$  is always parallel to the generating curve  $\mathcal{V}$ .<sup>1</sup> Then, the length from  $\mathbf{y}$  to  $\mathcal{C}(\mathbf{p}_f)$  is defined as the length of  $\mathcal{V}_p$  rather than  $\mathcal{V}_y$ , which is denoted by  $l(\mathbf{y})$ . Here  $\mathcal{V}_p$  is

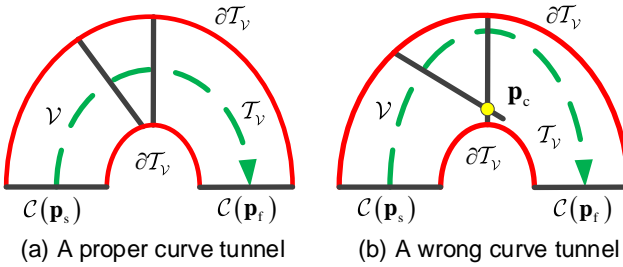


Figure 4. Proper and wrong curve virtual tubes.

a part of  $\mathcal{V}$  from  $\mathbf{p}$  to  $\mathbf{p}_f$ . According to this definition, it is obvious that points in the same cross section have the same length as  $\mathcal{C}(\mathbf{p}_f)$ , namely  $l(\mathbf{y}) = l(\mathbf{p})$ . If  $\mathbf{y}$  locates at front (back) of  $\mathcal{C}(\mathbf{p}_f)$ , the corresponding length is positive (negative). When  $\mathcal{C}(\mathbf{y}) = \mathcal{C}(\mathbf{p}_f)$ , the length is zero.

Then, an assumption is made on the proposed curve virtual tube.

**Assumption 1.** For any  $\mathbf{p}' \in \mathcal{T}_V$ , there exists a unique  $\mathbf{p} \in \mathcal{V}$  such that  $\mathbf{p}' \in \mathcal{C}(\mathbf{p})$ . Besides,  $\lambda_l(\mathbf{p}')$ ,  $\lambda_r(\mathbf{p}')$ ,  $\mathbf{t}_c(\mathbf{p}')$ ,  $\mathbf{t}_l(\mathbf{p}')$ ,  $\mathbf{t}_r(\mathbf{p}')$  are all continuous and differentiable.

*Assumption 1* implies that, any  $\mathbf{p}' \in \mathcal{T}_V$  has a unique direction to move. The generating curve and two curves of the tube boundary are also smooth. A tube satisfying *Assumption 1* is called a *proper tube*. As shown in Figure 4, the boundaries of two curve virtual tubes are the same, but they are two different curve virtual tubes because of different generating curves. The curve virtual tube shown in Figure 4(a) is a proper tube, while the curve virtual tube shown in Figure 4(b) is not because  $\mathbf{p}_c$  is an intersection point of two different cross sections. This implies that there are at least two different cross sections including  $\mathbf{p}_c$ . The following proposition gives a way for any  $\mathbf{p}' \in \mathcal{T}_V$  to get its unique moving direction.

**Proposition 1.** Under *Assumption 1*, for any  $\mathbf{p}' \in \mathcal{T}_V$ ,  $\mathbf{p} \in \mathcal{V}$ , if and only if

$$(\mathbf{p}' - \mathbf{p})^T \mathbf{t}_c(\mathbf{p}) = 0,$$

then  $\mathbf{p}' \in \mathcal{C}(\mathbf{p})$ .

*Proof.* It is easy to prove by following the definition of  $\mathcal{T}_V$  and *Assumption 1*.  $\square$

### 2.3 Two Areas around a Robot

Similarly to our previous work Quan et al. (2021a), Quan et al. (2021b), two types of circular areas around a robot used for avoidance control, namely safety area and avoidance area, are introduced. As shown in Figure 5, at the time  $t > 0$ , the *safety area*  $\mathcal{S}_i$  of the  $i$ th robot is defined as

$$\mathcal{S}_i(t) = \{\mathbf{x} \in \mathbb{R}^2 : \|\mathbf{x} - \mathbf{p}_i(t)\| \leq r_s\},$$

where  $r_s > 0$  is the *safety radius*. For all robots, no conflict with each other implies that  $\mathcal{S}_i \cap \mathcal{S}_j = \emptyset$ , namely  $\|\mathbf{p}_i - \mathbf{p}_j\| > 2r_s$ , where  $i, j = 1, \dots, M, i \neq j$ . Besides, the *avoidance area* is defined for starting the avoidance control. As shown in Figure 5, at the time  $t > 0$ , the avoidance area  $\mathcal{A}_i$  of the  $i$ th robot is defined as

$$\mathcal{A}_i(t) = \{\mathbf{x} \in \mathbb{R}^2 : \|\mathbf{x} - \mathbf{p}_i(t)\| \leq r_a\},$$

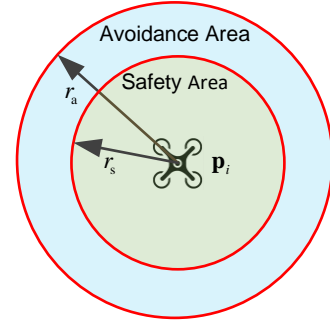


Figure 5. Safety area and avoidance area.

where  $r_a > 0$  is the *avoidance radius*. For collision avoidance with a pair of robots, if there exists  $\mathcal{A}_i \cap \mathcal{S}_j \neq \emptyset$  and  $\mathcal{A}_j \cap \mathcal{S}_i \neq \emptyset$ , namely  $\|\mathbf{p}_i - \mathbf{p}_j\| \leq r_a + r_s$ , then the  $i$ th and  $j$ th robots should avoid each other. The set  $\mathcal{N}_{m,i}$  is defined as the collection of all mark numbers of other robots whose safety areas have intersection with the avoidance area of the  $i$ th robot, namely

$$\mathcal{N}_{m,i} = \{j : \mathcal{A}_i \cap \mathcal{S}_j \neq \emptyset\},$$

where  $i, j = 1, \dots, M, i \neq j$ . Besides, when the  $j$ th robot or the tube boundary just enters the avoidance area  $\mathcal{A}_i$  of the  $i$ th robot, it is required that there be no conflict in the beginning. Therefore, at least we set that  $r_a > r_s$ .

### 2.4 Problem Formulation

With the descriptions above, some extra assumptions are imposed to get the main problem of this paper.

**Assumption 2.** The initial condition of the  $i$ th robot satisfies  $\mathcal{S}_i(0) \subset \mathcal{T}_V$ , and  $l(\mathbf{p}_i(0)) < 0, i = 1, \dots, M$ , namely all robots with their safety areas are inside the curve virtual tube and all robots locate at back of the finishing line  $\mathcal{C}(\mathbf{p}_f)$  in the beginning.

**Assumption 3.** The robots' initial conditions satisfy  $\mathcal{S}_i(0) \cap \mathcal{S}_j(0) = \emptyset$ , namely  $\|\mathbf{p}_i(0) - \mathbf{p}_j(0)\| > 2r_s$ , where  $i, j = 1, \dots, M, i \neq j$ .

**Assumption 4.** Once a robot arrives at the finishing line  $\mathcal{C}(\mathbf{p}_f)$ , it will quit this curve virtual tube not to affect other robots behind. Mathematically, given a constant  $\epsilon_0 > 0$ , a robot arrives near the finishing line  $\mathcal{C}(\mathbf{p}_f)$  if

$$l(\mathbf{p}_i) \geq -\epsilon_0. \quad (3)$$

Based on *Assumptions 1-4* above, the *curve virtual tube passing problem* is stated in the following.

**Curve virtual tube passing problem.** Under *Assumptions 1-4*, design the velocity command  $\mathbf{v}_{c,i}$  to guide all robots to pass through the curve virtual tube  $\mathcal{T}_V$ , meanwhile avoiding colliding with each other ( $\mathcal{S}_i(t) \cap \mathcal{S}_j(t) = \emptyset$ ) and keeping within the tube ( $\mathcal{S}_i(t) \cap \partial\mathcal{T}_V = \emptyset$ ), where  $i, j = 1, \dots, M, i \neq j, t > 0$ .

## 3 Preliminaries

### 3.1 Line Integrals of Vector Fields

In order to make this paper self-contained, the concept about line integrals of vector fields is introduced (Thomas et al. 2003, pp. 901-911). Suppose that  $f(x, y)$  is a real-valued

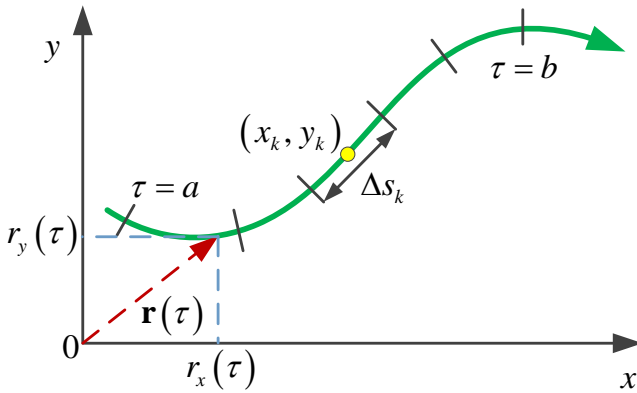


**Figure 6.** The curve  $\mathbf{r}(\tau)$  is partitioned into small arcs from  $\tau = a$  to  $\tau = b$ . The length of a typical subarc is  $\Delta s_k$ .

function. We wish to integrate this function over a curve  $\mathcal{V}$  lying within the domain of  $f$ , which is parameterized by  $\mathbf{r}(\tau) = [r_x(\tau) \ r_y(\tau)]^T$ ,  $a \leq \tau \leq b$ . Then, the values of  $f$  along the curve are given by a composite function  $f(r_x(\tau), r_y(\tau))$ . We are going to integrate this composite function with respect to the arc length from  $\tau = a$  to  $\tau = b$ .

As shown in Figure 6, given a finite number  $n$ , the curve  $\mathcal{V}$  is partitioned into  $n$  subarcs. The length of the typical  $k$ th subarc is  $\Delta s_k$ . In each subarc, we choose a point  $(x_k, y_k)$  and a sum is formed as

$$S_n = \sum_{k=1}^n f(x_k, y_k) \Delta s_k,$$

which is similar to a Riemann sum. Depending on how we partition the curve  $\mathcal{V}$  and pick  $(x_k, y_k)$  in the  $k$ th subarc, we may get different values for  $S_n$ . If  $f$  is continuous and the functions  $r_x(\tau)$  and  $r_y(\tau)$  have continuous first derivatives, these sums approach a limit as  $n$  increases, meanwhile the lengths  $\Delta s_k$  approach zero. This limit gives the following definition, similar to that for a single integral. In the definition, it is assumed that the partition satisfies  $\Delta s_k \rightarrow 0$  as  $n \rightarrow \infty$ .

**Definition 1.** If  $f$  is defined on a curve  $\mathcal{V}$  given parametrically by  $\mathbf{r}(\tau)$ ,  $a \leq \tau \leq b$ , then the line integral of  $f$  over  $\mathcal{V}$  is expressed as  $\int_{\mathcal{V}} f(x, y) ds$ .

The parametrization  $\mathbf{r}(\tau)$  defines a direction along  $\mathcal{V}$ , which is called as the forward direction. At each point along the curve  $\mathcal{V}$ , the tangent vector

$$\mathbf{t}_c = \frac{d\mathbf{r}}{ds} \quad (4)$$

is a unit vector tangent pointing in the *forward direction*. Intuitively, the line integral of the vector field  $\mathbf{f}$  is the line integral of the scalar tangential component of  $\mathbf{f}$  along  $\mathcal{V}$ . This tangential component is given by

$$\mathbf{f}^T \mathbf{t}_c = \frac{\mathbf{f}^T d\mathbf{r}}{ds}. \quad (5)$$

Then, according to *Definition 1*, the line integral of  $\mathbf{f}$  along  $\mathcal{V}$  is shown as

$$\int_{\mathcal{V}} \mathbf{f}^T \mathbf{t}_c ds = \int_{\mathcal{V}} \frac{\mathbf{f}^T d\mathbf{r}}{ds} ds = \int_{\mathcal{V}} \mathbf{f}^T d\mathbf{r}.$$

Evaluate the line integral with respect to the parameter  $a \leq \tau \leq b$  and it is obtained that

$$\int_{\mathcal{V}} \mathbf{f}^T d\mathbf{r} = \int_a^b \mathbf{f}(\mathbf{r}(\tau))^T \frac{d\mathbf{r}(\tau)}{d\tau} d\tau. \quad (6)$$

### 3.2 Line Integral Lyapunov Function

Given a specific point  $\mathbf{p} \in \mathcal{V}$ , its length to  $\mathcal{C}(\mathbf{p}_f)$  is expressed as

$$l(\mathbf{p}) = \int_{\mathcal{V}_{\mathbf{p}}} dl(\mathbf{x}).$$

According to (4) and (5), there exists

$$dl(\mathbf{x}) = \mathbf{t}_c^T(\mathbf{x}) d\mathbf{x},$$

where  $dl(\mathbf{x})$  is an increased length at  $\mathbf{x} \in \mathcal{V}$ . Then given a general point  $\mathbf{y} \in \mathcal{V}_{\mathbf{p}}$ , its length to  $\mathcal{C}(\mathbf{p}_f)$  is similarly defined as

$$l(\mathbf{y}) = \int_{\mathcal{V}_{\mathbf{y}}} dl(\mathbf{x}),$$

where  $dl(\mathbf{x})$  is an increased length at  $\mathbf{x} \in \mathcal{V}_{\mathbf{y}}$ . However, as shown in Figure 3, the increased length of  $\mathcal{V}_{\mathbf{y}}$  projected on  $\mathcal{V}_{\mathbf{p}}$  has to multiply by  $\eta(\mathbf{x})$ , which is a scaling factor satisfying  $0 < \eta_{\min} < \eta(\mathbf{x}) < \eta_{\max} < \infty$ . Hence, it is obtained that

$$dl(\mathbf{x}) = \eta(\mathbf{x}) \mathbf{t}_c^T(\mathbf{x}) d\mathbf{x}. \quad (7)$$

It should be noted that when  $\mathcal{V}_{\mathbf{y}}$  is shorter than  $\mathcal{V}_{\mathbf{p}}$ , there exists  $\eta(\mathbf{x}) < 1$ , otherwise  $\eta(\mathbf{x}) \geq 1$ .

Then, a line integral Lyapunov function for vectors is defined as

$$V_{li}(\mathbf{y}) = \int_{\mathcal{V}_{\mathbf{y}}} \text{sat}(k_1 l(\mathbf{x}) \eta(\mathbf{x}) \mathbf{t}_c(\mathbf{x}), v_{m,i})^T d\mathbf{x}, \quad (8)$$

where  $k_1 > 0$ . In the following lemma, its properties will be shown.

**Lemma 1.** Suppose that the line integral Lyapunov function  $V_{li}(\mathbf{y})$  is defined as (8). Then it is obtained that (i)  $V_{li}(\mathbf{y}) > 0$  if  $|l(\mathbf{y})| \neq 0$ ; (ii) if  $\|\mathbf{y}\| \rightarrow \infty$ , then  $V_{li}(\mathbf{y}) \rightarrow \infty$ ; (iii) if  $V_{li}(\mathbf{y})$  is bounded, then  $\|\mathbf{y}\|$  is bounded.

*Proof.* See Appendix.  $\square$

### 3.3 Single Panel Method

Panel methods are widely used in aerodynamics calculations to obtain the solution to the potential flow problem around arbitrarily shaped bodies [Rimon \(1990\)](#). Here the single panel method is used to represent the repulsive potential field of the tube boundary. Assume that there is a line segment  $[\mathbf{a} + g_1 \mathbf{t}, \mathbf{a} + g_2 \mathbf{t}]$ ,  $\|\mathbf{t}\| = 1$ ,  $g_1, g_2 \in \mathbb{R}$ , the potential at any point  $\mathbf{p}$  induced by the sources contained within a small element  $d\mathbf{x}$  is shown as

$$d\phi = \ln(\|\mathbf{p} - (\mathbf{a} + x\mathbf{t})\| - d) d\mathbf{x},$$

where  $d \geq 0$  is a threshold distance. The induced repulsive potential function by the whole panel  $[\mathbf{a} + g_1 \mathbf{t}, \mathbf{a} + g_2 \mathbf{t}]$  is expressed as

$$\phi(\mathbf{p}, \mathbf{a}, \mathbf{t}, g_1, g_2, d) = \int_{g_1}^{g_2} \ln(\|\mathbf{p} - (\mathbf{a} + x\mathbf{t})\| - d) dx. \quad (9)$$

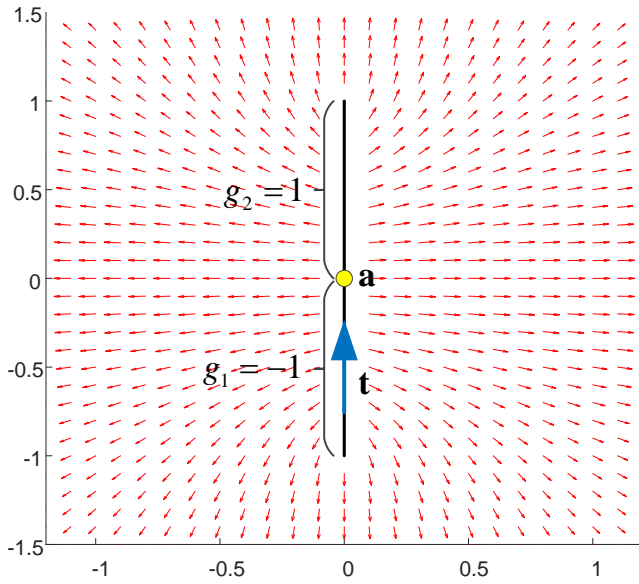


**Figure 7.** Vector field of a single panel [Rimon \(1990\)](#).

Given  $\mathbf{a} = [0 \ 0]^T$ ,  $\mathbf{t} = [0 \ 1]^T$ ,  $g_1 = -1$ ,  $g_2 = 1$ ,  $d = 0$ , the corresponding negative vector field  $-\partial\phi/\partial\mathbf{p}$  is shown in Figure 7. It can be seen that the orientation is orthogonal to the line segment  $[\mathbf{a} + g_1\mathbf{t}, \mathbf{a} + g_2\mathbf{t}]$  when the point  $\mathbf{p}$  locates at the line  $y = 0$ . The orientation is parallel to  $[\mathbf{a} + g_1\mathbf{t}, \mathbf{a} + g_2\mathbf{t}]$  when the point  $\mathbf{p}$  locates at the line  $x = 0$ . As the potential function  $\phi$  is smooth and differentiable, the orientation of the vector field also changes smoothly. This phenomenon is important for the proof of no deadlock in the following.

### 3.4 Two Smooth Functions

Two smooth functions are defined for the design of Lyapunov-like barrier functions in the following [Panagou et al. \(2015\)](#). As shown in Figure 8 (upper plot), the first is a second-order differentiable “bump” function

$$\sigma(x, d_1, d_2) = \begin{cases} 1 & x \leq d_1 \\ Ax^3 + Bx^2 + Cx + D & d_1 \leq x \leq d_2 \\ 0 & d_2 \leq x \end{cases} \quad (10)$$

with  $A = -2/(d_1 - d_2)^3$ ,  $B = 3(d_1 + d_2)/(d_1 - d_2)^3$ ,  $C = -6d_1d_2/(d_1 - d_2)^3$ ,  $D = d_2^2(3d_1 - d_2)/(d_1 - d_2)^3$ . The derivative of  $\sigma(x, d_1, d_2)$  with respect to  $x$  is

$$\frac{\partial\sigma(x, d_1, d_2)}{\partial x} = \begin{cases} 0 & x \leq d_1 \\ 3Ax^2 + 2Bx + C & d_1 \leq x \leq d_2 \\ 0 & d_2 \leq x \end{cases}.$$

As shown in Figure 8 (lower plot), to approximate a saturation function

$$\bar{s}(x) = \min(x, 1), x \geq 0,$$

the other is a smooth saturation function

$$s(x, \epsilon_s) = \begin{cases} x & 0 \leq x \leq x_1 \\ (1 - \epsilon_s) + \sqrt{\epsilon_s^2 - (x - x_2)^2} & x_1 \leq x \leq x_2 \\ 1 & x_2 \leq x \end{cases}$$

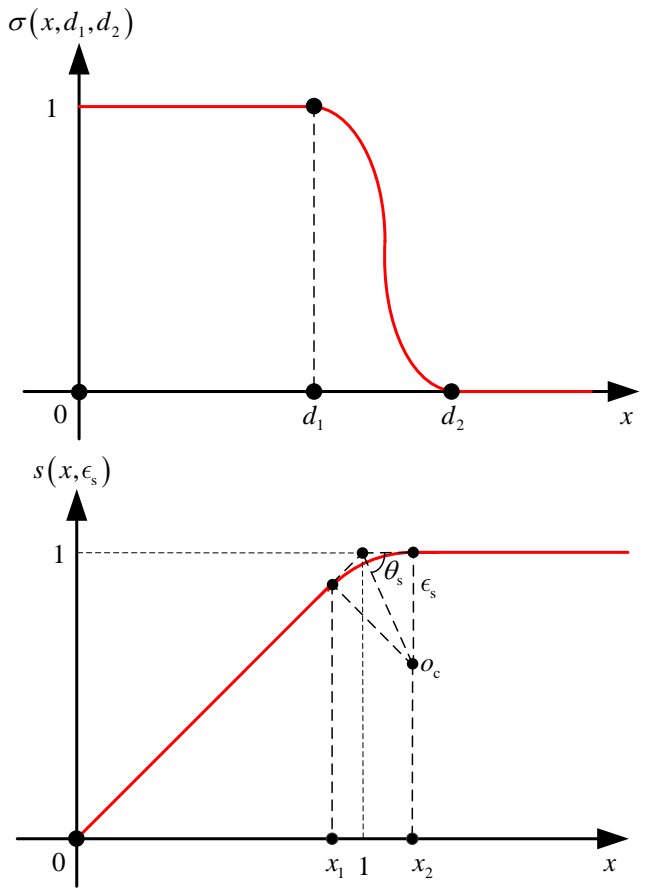


**Figure 8.** Two smooth functions. For a smooth saturation function,  $\theta_s = 67.5^\circ$ .

with  $x_2 = 1 + \frac{1}{\tan 67.5^\circ} \epsilon_s$  and  $x_1 = x_2 - \sin 45^\circ \epsilon_s$ . Since it is required  $x_1 > 0$ , one has  $\epsilon_s \leq \frac{\tan 67.5^\circ}{\tan 67.5^\circ \sin 45^\circ - 1}$ . For any  $\epsilon_s \in \left[0, \frac{\tan 67.5^\circ}{\tan 67.5^\circ \sin 45^\circ - 1}\right]$ , it is easy to see

$$s(x, \epsilon_s) \leq \bar{s}(x)$$

and

$$\limsup_{\epsilon_s \rightarrow 0} \sup_{x \geq 0} |\bar{s}(x) - s(x, \epsilon_s)| = 0.$$

The derivative of  $s(x, \epsilon_s)$  with respect to  $x$  is

$$\frac{\partial s(x, \epsilon_s)}{\partial x} = \begin{cases} \frac{1}{\sqrt{\epsilon_s^2 - (x - x_2)^2}} & 0 \leq x \leq x_1 \\ \frac{x_2 - x}{\sqrt{\epsilon_s^2 - (x - x_2)^2}} & x_1 \leq x \leq x_2 \\ 0 & x_2 \leq x \end{cases}.$$

For any  $\epsilon_s > 0$ , we have  $\sup_{x \geq 0} |\partial s(x, \epsilon_s) / \partial x| \leq 1$ .

## 4 Distributed Robotic Swarm Control for Passing through a Curve Virtual Tube

### 4.1 Line Integral Lyapunov Function for Approaching Finishing Line

Define  $\mathcal{V}_{\mathbf{p}_i}$  to be the curve from  $\mathbf{p}_i$  to  $\mathcal{C}(\mathbf{p}_f)$  along the tangent direction  $\mathbf{t}_c(\cdot) \in \mathbb{R}^2$ , which is always parallel to  $\mathcal{V}$ . According to (8), a line integral Lyapunov function is defined as

$$V_{1,i} = \int_{\mathcal{V}_{\mathbf{p}_i}} \text{sat}(k_1 l(\mathbf{x}) \eta(\mathbf{x}) \mathbf{t}_c(\mathbf{x}), v_{m,i})^T d\mathbf{x}, \quad (11)$$

where  $i = 1, 2, \dots, M$ . According to (6), evaluate the line integral with respect to the parameter  $t$  and it can be obtained that

$$\begin{aligned} V_{i,i} &= \int_0^t \text{sat}(k_1 l(\mathbf{p}_i) \eta(\mathbf{p}_i) \mathbf{t}_c(\mathbf{p}_i), v_{m,i})^T \dot{\mathbf{p}}_i d\tau \\ &= \int_0^t \text{sat}(k_1 l(\mathbf{p}_i) \eta(\mathbf{p}_i) \mathbf{t}_c(\mathbf{p}_i), v_{m,i})^T \mathbf{v}_{c,i} d\tau. \end{aligned} \quad (12)$$

The objective of the designed velocity command is to make  $V_{i,i}$  approach zero. This implies that  $|l(\mathbf{p}_i)| = 0$  according to *Lemma 1*, namely the  $i$ th robot has arrived at the finishing line  $\mathcal{C}(\mathbf{p}_f)$ .

## 4.2 Barrier Function for Avoiding Conflict

Define a position error between the  $i$ th and  $j$ th robot, which is shown as

$$\tilde{\mathbf{p}}_{m,ij} \triangleq \mathbf{p}_i - \mathbf{p}_j.$$

With the definition above, its derivative is

$$\dot{\tilde{\mathbf{p}}}_{m,ij} = \mathbf{v}_{c,i} - \mathbf{v}_{c,j}.$$

According to two smooth functions, the barrier function for the  $i$ th robot avoiding conflict with the  $j$ th robot is defined as

$$V_{m,ij} = \frac{k_2 \sigma_m(\|\tilde{\mathbf{p}}_{m,ij}\|)}{(1 + \epsilon_m) \|\tilde{\mathbf{p}}_{m,ij}\| - 2r_s s \left( \frac{\|\tilde{\mathbf{p}}_{m,ij}\|}{2r_s}, \epsilon_s \right)}, \quad (13)$$

where  $k_2, \epsilon_m, \epsilon_s > 0$ . Based on the definitions of the safety area and the avoidance area, the smooth function  $\sigma(\cdot)$  in (10) is defined as  $\sigma_m(x) \triangleq \sigma(x, 2r_s, r_a + r_s)$ . The function  $V_{m,ij}$  has the following properties.

- (i)  $\partial V_{m,ij} / \partial \|\tilde{\mathbf{p}}_{m,ij}\| \leq 0$  as  $V_{m,ij}$  is a nonincreasing function with respect to  $\|\tilde{\mathbf{p}}_{m,ij}\|$ .
- (ii) If  $\|\tilde{\mathbf{p}}_{m,ij}\| > r_s + r_a$ , namely  $\mathcal{A}_i \cap \mathcal{S}_j \neq \emptyset$  and  $\mathcal{A}_j \cap \mathcal{S}_i \neq \emptyset$ , then  $V_{m,ij} = 0$  and  $\partial V_{m,ij} / \partial \|\tilde{\mathbf{p}}_{m,ij}\| = 0$ ; if  $V_{m,ij} = 0$ , then  $\|\tilde{\mathbf{p}}_{m,ij}\| > r_s + r_a > 2r_s$ .
- (iii) If  $0 < \|\tilde{\mathbf{p}}_{m,ij}\| < 2r_s$ , namely  $\mathcal{S}_i \cap \mathcal{S}_j \neq \emptyset$  (they may not collide in practice), then there exists a sufficiently small  $\epsilon_s > 0$  such that

$$V_{m,ij} = \frac{k_2}{\epsilon_m \|\tilde{\mathbf{p}}_{m,ij}\|} \geq \frac{k_2}{2\epsilon_m r_s}.$$

The objective of the designed velocity command is to make  $V_{m,ij}$  zero or as small as possible, which implies that  $\|\tilde{\mathbf{p}}_{m,ij}\| > 2r_s$  according to property (ii), namely the  $i$ th robot will not conflict with the  $j$ th robot.

## 4.3 Barrier Functions for Keeping within Curve Virtual Tube

**4.3.1 Algebraic Description for any Robot with its Safety Area inside the Curve Virtual Tube** When the  $i$ th robot with its safety area  $\mathcal{S}_i$  is moving inside the curve virtual tube, namely  $\mathcal{S}_i \subset \mathcal{T}_V$ ,  $\mathcal{S}_i$  is actually confined between the crossing sections  $\mathcal{C}(\mathbf{p}_s^-(\mathbf{p}_i))$  and  $\mathcal{C}(\mathbf{p}_s^+(\mathbf{p}_i))$  as shown in Figure 9, where two points  $\mathbf{p}_s^-(\mathbf{p}_i), \mathbf{p}_s^+(\mathbf{p}_i) \in \mathcal{V}$  with respect to  $\mathbf{p}_i$  and  $r_s$  are defined as

$$\begin{aligned} \mathbf{p}_s^-(\mathbf{p}_i) &\triangleq \underset{\mathbf{x} \in \mathcal{V}, \text{dist}(\mathbf{p}_i, \mathcal{C}(\mathbf{x})) < r_s}{\text{argmin}} l(\mathbf{x}), \\ \mathbf{p}_s^+(\mathbf{p}_i) &\triangleq \underset{\mathbf{x} \in \mathcal{V}, \text{dist}(\mathbf{p}_i, \mathcal{C}(\mathbf{x})) < r_s}{\text{argmax}} l(\mathbf{x}), \end{aligned}$$

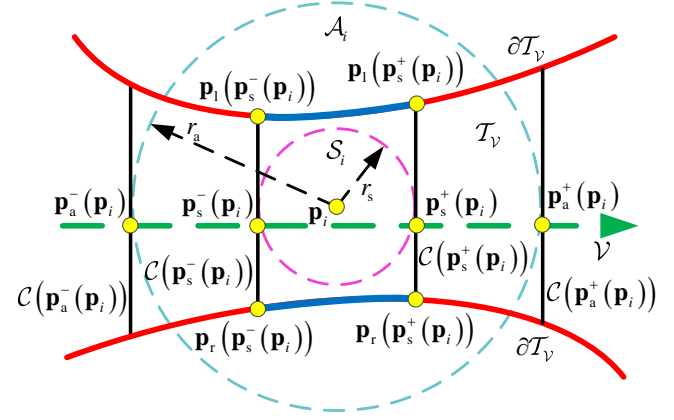


**Figure 9.** A visual representation about  $\mathcal{S}_i \subset \mathcal{T}_V$ . This requires  $\text{dist}(\mathbf{p}_i, \partial \mathcal{T}_V \cap \mathcal{C}(\mathbf{p}')) > r_s$  if  $l(\mathbf{p}') > l(\mathbf{p}_s^-(\mathbf{p}_i))$  or  $l(\mathbf{p}') < l(\mathbf{p}_s^+(\mathbf{p}_i))$ , namely  $\mathcal{S}_i$  should have no intersection with the curves in blue, which are parts of  $\partial \mathcal{T}_V$  from  $\mathbf{p}_l(\mathbf{p}_s^-(\mathbf{p}_i))$  to  $\mathbf{p}_l(\mathbf{p}_s^+(\mathbf{p}_i))$  and from  $\mathbf{p}_r(\mathbf{p}_s^-(\mathbf{p}_i))$  to  $\mathbf{p}_r(\mathbf{p}_s^+(\mathbf{p}_i))$ .

where the function  $\text{dist}(\cdot)$  is defined as the Euclidean distance. Obviously, the point  $\mathbf{p}_s^-(\mathbf{p}_i)$  locates at back of  $\mathbf{p}_i$ , and the point  $\mathbf{p}_s^+(\mathbf{p}_i)$  locates at front of  $\mathbf{p}_i$ . For the  $i$ th robot, the set  $\mathcal{V}_{s,i}$  is defined as the collection of all points on the generating curve whose lengths are between  $l(\mathbf{p}_s^-(\mathbf{p}_i))$  and  $l(\mathbf{p}_s^+(\mathbf{p}_i))$ , namely

$$\mathcal{V}_{s,i} = \{\mathbf{x} \in \mathcal{V} : l(\mathbf{x}) \in (l(\mathbf{p}_s^-(\mathbf{p}_i)), l(\mathbf{p}_s^+(\mathbf{p}_i)))\},$$

where  $i = 1, \dots, M$ . Then an algebraic description for the  $i$ th robot with its safety area inside the curve virtual tube, namely  $\mathcal{S}_i \subset \mathcal{T}_V$ , is expressed as

$$\text{dist}(\mathbf{p}_i, \partial \mathcal{T}_V \cap \mathcal{C}(\mathbf{p}')) > r_s, \forall \mathbf{p}' \in \mathcal{V}_{s,i}. \quad (14)$$

Besides, two points  $\mathbf{p}_a^-(\mathbf{p}_i), \mathbf{p}_a^+(\mathbf{p}_i) \in \mathcal{V}$  with respect to  $\mathbf{p}_i$  and  $r_a$  are similarly defined as

$$\begin{aligned} \mathbf{p}_a^-(\mathbf{p}_i) &\triangleq \underset{\mathbf{x} \in \mathcal{V}, \text{dist}(\mathbf{p}_i, \mathcal{C}(\mathbf{x})) < r_a}{\text{argmin}} l(\mathbf{x}), \\ \mathbf{p}_a^+(\mathbf{p}_i) &\triangleq \underset{\mathbf{x} \in \mathcal{V}, \text{dist}(\mathbf{p}_i, \mathcal{C}(\mathbf{x})) < r_a}{\text{argmax}} l(\mathbf{x}). \end{aligned}$$

Obviously, the point  $\mathbf{p}_a^-(\mathbf{p}_i)$  locates at back of  $\mathbf{p}_s^-(\mathbf{p}_i)$ , and the point  $\mathbf{p}_a^+(\mathbf{p}_i)$  locates at front of  $\mathbf{p}_s^+(\mathbf{p}_i)$ . For the  $i$ th robot, the set  $\mathcal{V}_{a,i}$  is defined as the collection of all points on the generating curve whose lengths are between  $l(\mathbf{p}_a^-(\mathbf{p}_i))$  and  $l(\mathbf{p}_a^+(\mathbf{p}_i))$ , namely

$$\mathcal{V}_{a,i} = \{\mathbf{x} \in \mathcal{V} : l(\mathbf{x}) \in (l(\mathbf{p}_a^-(\mathbf{p}_i)), l(\mathbf{p}_a^+(\mathbf{p}_i)))\},$$

where  $i = 1, \dots, M$ .

**4.3.2 Barrier Functions Design with Single Panel Method** As shown in Figure 10, for any  $\mathbf{p} \in \mathcal{V}$ , two extended straight-line tube boundaries are defined

$$\begin{aligned} &[\mathbf{p}_l(\mathbf{p}) + l_r(\mathbf{p}) \mathbf{t}_l(\mathbf{p}), \mathbf{p}_l(\mathbf{p}) + l_l(\mathbf{p}) \mathbf{t}_l(\mathbf{p})], \\ &[\mathbf{p}_r(\mathbf{p}) + r_r(\mathbf{p}) \mathbf{t}_r(\mathbf{p}), \mathbf{p}_r(\mathbf{p}) + r_l(\mathbf{p}) \mathbf{t}_r(\mathbf{p})], \end{aligned}$$

satisfying

$$\begin{aligned} l_r(\mathbf{p}), r_r(\mathbf{p}) &> 0, \\ l_l(\mathbf{p}), r_l(\mathbf{p}) &< 0. \end{aligned}$$

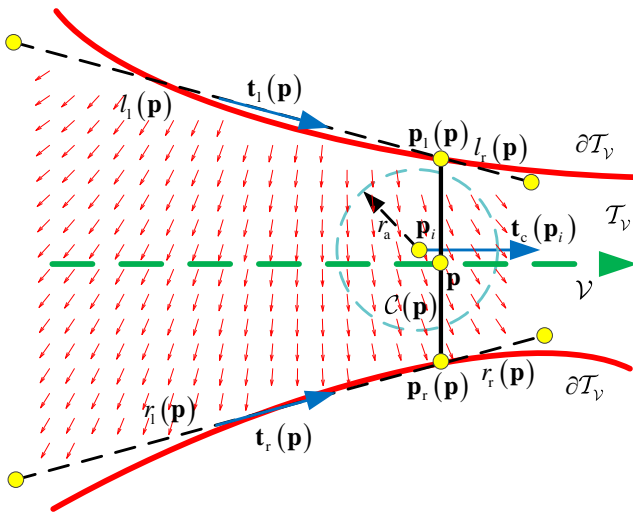


**Figure 10.** Relative concepts of two extended tube boundaries. Red arrows represent the negative vector field of the single panel  $[p_l(p) + l_l(p)t_l(p), p_l(p) + l_l(p)t_l(p)]$ , namely  $-(\partial\phi_l(p_i, p)/\partial p_i)^T$ . In this figure, there exists  $-t_c^T(p_i)(\partial\phi_l(p_i, p)/\partial p_i)^T > 0$

According to the potential function of the single panel (9), the potential fields of the two extended tube boundaries at  $p_i \in \mathcal{T}_v$  are shown as

$$\begin{aligned} \phi(p_i, p_l(p), t_l(p), l_l(p), l_l(p), r_s), \\ \phi(p_i, p_r(p), t_r(p), r_r(p), r_l(p), r_s), \end{aligned}$$

which will be written as  $\phi_l(p_i, p)$  and  $\phi_r(p_i, p)$  for short in the following. If there exists  $\text{dist}(p_i, C(p)) < r_a$ ,  $l_r(p), l_l(p), r_r(p), r_l(p)$  must satisfy the following constraints

$$-t_c^T(p_i) \left( \frac{\partial\phi_l(p_i, p)}{\partial p_i} \right)^T \geq 0, \quad (15)$$

$$-t_c^T(p_i) \left( \frac{\partial\phi_r(p_i, p)}{\partial p_i} \right)^T \geq 0. \quad (16)$$

Then, two barrier functions for achieving (14), namely the  $i$ th robot with its safety area keep within the tube, are defined as

$$V_{\text{tl},i} = k_3 \sum_{p \in \mathcal{V}_{a,i}} \phi_l(p_i, p), \quad (17)$$

$$V_{\text{tr},i} = k_3 \sum_{p \in \mathcal{V}_{a,i}} \phi_r(p_i, p), \quad (18)$$

where  $k_3 > 0$ . According to the constraints (15) and (16), there exists

$$\begin{cases} -t_c^T(p_i) \left( \frac{\partial V_{\text{tl},i}}{\partial p_i} \right)^T \geq 0 \\ -t_c^T(p_i) \left( \frac{\partial V_{\text{tr},i}}{\partial p_i} \right)^T \geq 0 \end{cases}. \quad (19)$$

The inequalities (19) mean that the angles between negative gradient directions of  $V_{\text{tl},i}, V_{\text{tr},i}$  inside the tube and the moving direction  $t_c(p_i)$  must keep smaller than  $90^\circ$ , which plays a crucial role in the stability proof. The objective of the

designed velocity command is to make  $V_{\text{tl},i}, V_{\text{tr},i}$  as small as possible, which implies that the  $i$ th robot will keep within the tube.

**Remark 1.** In (17) and (18), the reason for applying  $\mathcal{V}_{a,i}$  rather than  $\mathcal{V}_{s,i}$  is to prevent the robot from moving outside the curve virtual tube as there may exist unpredictable uncertainties out of the assumptions we make.

#### 4.4 Swarm Controller Design

Let  $\mathbf{p}$  be the collection  $(p_1, \dots, p_M)$ . The velocity command of the  $i$ th robot is designed as

$$\mathbf{v}_{c,i} = \mathbf{v}(\mathcal{T}_v, p_i, \mathbf{p}, r_s), \quad (20)$$

where

$$\begin{aligned} \mathbf{v}(\mathcal{T}_v, p_i, \mathbf{p}, r_s) \triangleq -\text{sat} \left( \underbrace{\text{sat}(k_1 l(p_i) \eta(p_i) t_c(p_i), v_{m,i})}_{\text{Line Approaching}} \right. \\ \left. + \underbrace{\sum_{j \in \mathcal{N}_{m,i}} -b_{ij} \tilde{\mathbf{p}}_{m,ij} + \left( \frac{\partial V_{\text{tl},i}}{\partial p_i} \right)^T + \left( \frac{\partial V_{\text{tr},i}}{\partial p_i} \right)^T, v_{m,i}}_{\text{Virtual Tube Keeping}} \right) \end{aligned}$$

with<sup>2</sup>

$$b_{ij} = -\frac{\partial V_{m,ij}}{\partial \|\tilde{\mathbf{p}}_{m,ij}\|} \frac{1}{\|\tilde{\mathbf{p}}_{m,ij}\|}.$$

This is a distributed control form. Unlike the formation control, neighboring robots' IDs of a robot are not required. With some active detection devices, such as cameras or radars, the proposed controller can work autonomously without wireless communication and other robots' IDs.

**Remark 2.** It is noticed that the velocity command (20) is saturated, whose norm cannot exceed  $v_{m,i}$ . If the case such as  $\|\tilde{\mathbf{p}}_{m,ij_1}\| < 2r_s$  happens in practice due to unpredictable uncertainties out of the assumptions we make, this may not imply that the  $i$ th robot has collided the  $j_1$ th UAV physically. In this case, the velocity command (20) degenerates to be

$$\begin{aligned} \mathbf{v}_{c,i} = -\text{sat} \left( \text{sat}(k_1 l(p_i) \eta(p_i) t_c(p_i), v_{m,i}) \right. \\ \left. - \sum_{j=1, j \neq i, j_1}^M b_{ij} \tilde{\mathbf{p}}_{m,ij} - b_{ij_1} \tilde{\mathbf{p}}_{m,ij_1} \right. \\ \left. + \left( \frac{\partial V_{\text{tl},i}}{\partial p_i} \right)^T + \left( \frac{\partial V_{\text{tr},i}}{\partial p_i} \right)^T, v_{m,i} \right)$$

with

$$b_{ij_1} \approx \frac{k_2}{\epsilon_m \|\tilde{\mathbf{p}}_{m,ij_1}\|^3}.$$

Since  $\epsilon_m$  is chosen to be sufficiently small, the term  $b_{ij_1} \tilde{\mathbf{p}}_{m,ij_1}$  will dominate<sup>3</sup> so that the velocity command  $\mathbf{v}_{c,i}$  becomes

$$\mathbf{v}_{c,i} \approx \text{sat} \left( \frac{k_2}{\epsilon_m \|\tilde{\mathbf{p}}_{m,ij_1}\|^3} \tilde{\mathbf{p}}_{m,ij_1}, v_{m,i} \right).$$

This implies that  $\|\tilde{\mathbf{p}}_{m,ij_1}\|$  will be increased very fast so that the  $i$ th robot can keep away from the  $j_1$ th robot immediately.

#### 4.5 Stability Analysis

In order to investigate the stability of the proposed controller for the curve virtual tube passing problem, a function is defined as follows

$$V = \sum_{i=1}^M \left( V_{l,i} + \frac{1}{2} \sum_{j=1, j \neq i}^M V_{m,ij} + V_{tl,i} + V_{tr,i} \right),$$

where  $V_{l,i}$ ,  $V_{m,ij}$ ,  $V_{tl,i}$ ,  $V_{tr,i}$  are defined in (11), (13), (17), (18) respectively. The derivative of  $V$  is shown as

$$\begin{aligned} \dot{V} &= \sum_{i=1}^M \left( \text{sat}(k_1 l(\mathbf{p}_i) \eta(\mathbf{p}_i) \mathbf{t}_c(\mathbf{p}_i), v_{m,i})^T \mathbf{v}_{c,i} \right. \\ &\quad \left. - \frac{1}{2} \sum_{j=1, j \neq i}^M b_{ij} \tilde{\mathbf{p}}_{m,ij}^T (\mathbf{v}_{c,i} - \mathbf{v}_{c,j}) + \frac{\partial V_{tl,i}}{\partial \mathbf{p}_i} \mathbf{v}_{c,i} + \frac{\partial V_{tr,i}}{\partial \mathbf{p}_i} \mathbf{v}_{c,i} \right) \\ &= \sum_{i=1}^M \left( \text{sat}(k_1 l(\mathbf{p}_i) \eta(\mathbf{p}_i) \mathbf{t}_c(\mathbf{p}_i), v_{m,i}) - \sum_{j \in \mathcal{N}_{m,i}} b_{ij} \tilde{\mathbf{p}}_{m,ij} \right. \\ &\quad \left. + \left( \frac{\partial V_{tl,i}}{\partial \mathbf{p}_i} \right)^T + \left( \frac{\partial V_{tr,i}}{\partial \mathbf{p}_i} \right)^T \right) \mathbf{v}_{c,i}, \end{aligned}$$

where

$$\sum_{j=1, j \neq i}^M b_{ij} \tilde{\mathbf{p}}_{m,ij} = \sum_{j \in \mathcal{N}_{m,i}} b_{ij} \tilde{\mathbf{p}}_{m,ij}.$$

By using the velocity command (20) for all robots,  $\dot{V}$  satisfies

$$\dot{V} \leq 0. \quad (21)$$

**Remark 3.** In fact, for approaching the finishing line, a straightforward and intuitive way is to define a Lyapunov function as

$$V'_{l,i} = \frac{1}{2} k_1 l^2(\mathbf{p}_i), \quad (22)$$

whose derivative is shown as

$$\dot{V}'_{l,i} = k_1 l(\mathbf{p}_i) \eta(\mathbf{p}_i) \mathbf{t}_c^T(\mathbf{p}_i) \mathbf{v}_{c,i}.$$

By replacing  $V_{l,i}$  in (11) with  $V'_{l,i}$  in (22),  $\dot{V}$  is converted as

$$\begin{aligned} \dot{V} &= \sum_{i=1}^M \left( k_1 l(\mathbf{p}_i) \eta(\mathbf{p}_i) \mathbf{t}_c(\mathbf{p}_i) - \sum_{j \in \mathcal{N}_{m,i}} b_{ij} \tilde{\mathbf{p}}_{m,ij} \right. \\ &\quad \left. + \left( \frac{\partial V_{tl,i}}{\partial \mathbf{p}_i} \right)^T + \left( \frac{\partial V_{tr,i}}{\partial \mathbf{p}_i} \right)^T \right) \mathbf{v}_{c,i}. \end{aligned}$$

In this way, we **CANNOT** introduce a *saturation* on the finishing line approaching term to the final controller. For such a purpose, the definition of the line integral Lyapunov function  $V_{l,i}$  in (11) is necessary.

Before the main result in this subsection is introduced, an important lemma is needed.

**Lemma 2.** Under Assumptions 1-4, suppose that (i) the velocity command for the  $i$ th robot is designed as (20); (ii) the curve virtual tube  $\mathcal{T}_V$  is wide enough for at least one robot to pass through. Then there exist sufficiently small  $\epsilon_m, \epsilon_s > 0$  in  $b_{ij}$  such that  $\mathcal{S}_i(t) \cap \mathcal{S}_j(t) = \emptyset$ ,  $\mathcal{S}_i(t) \cap \partial \mathcal{T}_V = \emptyset$ ,  $t \in [0, \infty)$  for all  $\mathbf{p}_i(0)$ ,  $i, j = 1, \dots, M$  and  $i \neq j$ .

*Proof.* See Appendix.  $\square$

With Lemmas 1-2 available, the main result is stated as follows.

**Theorem 1.** Under Assumptions 1-4, suppose that (i) the velocity command for the  $i$ th robot is designed as (20); (ii) given  $\epsilon_0 > 0$ , if (3) is satisfied, then  $b_{ij} \equiv 0$ ,  $(\partial V_{tl,i} / \partial \mathbf{p}_i)^T \equiv \mathbf{0}$ ,  $(\partial V_{tr,i} / \partial \mathbf{p}_i)^T \equiv \mathbf{0}$ , which implies that the  $i$ th robot is removed from the curve virtual tube  $\mathcal{T}_V$  mathematically; (iii) the curve virtual tube  $\mathcal{T}_V$  is wide enough for at least one robot to pass through. Then, there exist sufficiently small  $\epsilon_m, \epsilon_s > 0$  in  $b_{ij}$  and  $t_1 > 0$  such that all robots can satisfy (3) at  $t \geq t_1$ , meanwhile guaranteeing  $\mathcal{S}_i(t) \cap \mathcal{S}_j(t) = \emptyset$ ,  $\mathcal{S}_i(t) \cap \partial \mathcal{T}_V = \emptyset$ ,  $t \in [0, \infty)$  for all  $\mathbf{p}_i(0)$ ,  $i, j = 1, \dots, M$  and  $i \neq j$ .

*Proof.* See Appendix.  $\square$

#### 4.6 Modified Swarm Controller Design

However, the distributed controller (20) has two apparent imperfections in use.

- (i) The first problem is that any robot can approach the finishing line but its speed will slow down to zero. The reason is that  $l(\mathbf{p}_i) = 0$  when  $\mathbf{p}_i$  locates at  $\mathcal{C}(\mathbf{p}_f)$ .
- (ii) The second problem is that the values of  $l_r(\mathbf{p}), l_1(\mathbf{p}), r_r(\mathbf{p}), r_1(\mathbf{p})$  for all  $\mathbf{p} \in \mathcal{V}$  are difficult to obtain. The specific mathematical forms of  $\partial V_{tl,i} / \partial \mathbf{p}_i$  and  $\partial V_{tr,i} / \partial \mathbf{p}_i$  are also very complicated and inconvenient for practical use.

**4.6.1 Line Approaching Term with a Constant Speed** To solve the first problem, a modified finishing line  $\mathcal{C}(\mathbf{p}'_f)$  is defined as shown in Figure 11 with a length

$$l'(\mathbf{p}_i) = l(\mathbf{p}_i) - \rho,$$

where  $\rho \geq v_{m,i} / \eta_{\min}$ . In this case, the line approaching term becomes

$$\begin{aligned} &- \text{sat}(k_1 l'(\mathbf{p}_i) \eta(\mathbf{p}_i) \mathbf{t}_c(\mathbf{p}_i), v_{m,i}) \\ &= - \text{sat}(k_1 (l(\mathbf{p}_i) - \rho) \eta(\mathbf{p}_i) \mathbf{t}_c(\mathbf{p}_i), v_{m,i}) \\ &= v_{m,i} \mathbf{t}_c(\mathbf{p}_i). \end{aligned}$$

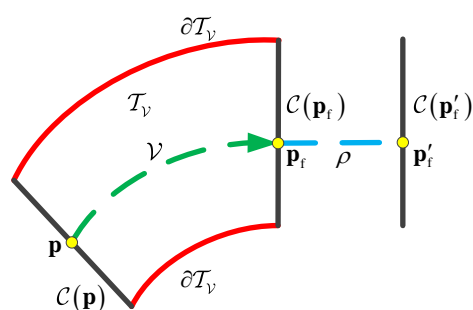


Figure 11. Modified Finishing Line.

**4.6.2 Unified Barrier Function for Keeping within Curve Virtual Tube** To solve the second problem, a unified barrier function is introduced to imitate the performance of  $V_{tl,i}$  and  $V_{tr,i}$ . An Euclidean distance error is defined between the  $i$ th robot and the tube boundary confined in  $\mathcal{C}(\mathbf{p}_i)$ , which is

shown as

$$d_{t,i} \triangleq r_t(\mathbf{p}_i) - \|\mathbf{p}_i - \mathbf{m}(\mathbf{p}_i)\|.$$

The derivative of this error is shown as

$$\dot{d}_{t,i} = \left( \frac{\partial r_t(\mathbf{p}_i)}{\partial \mathbf{p}_i} - \frac{(\mathbf{p}_i - \mathbf{m}(\mathbf{p}_i))^T}{\|\mathbf{p}_i - \mathbf{m}(\mathbf{p}_i)\|} \left( \mathbf{I}_2 - \frac{\partial \mathbf{m}(\mathbf{p}_i)}{\partial \mathbf{p}_i} \right) \right) \mathbf{v}_{c,i}.$$

For ensuring  $\mathcal{S}_i \cap \partial \mathcal{T}_V = \emptyset$ , at least it is required  $d_{t,i} > r_s$ . However, this constraint is not enough because the real distance from  $\mathbf{p}_i$  to  $\partial \mathcal{T}_V$  is usually smaller than  $d_{t,i}$  as shown in Figure 12. Hence a modified safety radius  $r'_s$  is proposed satisfying

$$r'_s = \inf_{\mathbf{x} \in \mathcal{V}} \text{dist}(\mathcal{C}(\mathbf{x}) \cap \mathcal{S}_{\mathcal{T}_V}, \partial \mathcal{T}_V) \quad (23)$$

and

$$\mathcal{S}_{\mathcal{T}_V} = \{\mathbf{x} \in \mathcal{T}_V : \text{dist}(\mathbf{x}, \partial \mathcal{T}_V) \geq r_s\}.$$

Then there exists the following proposition.

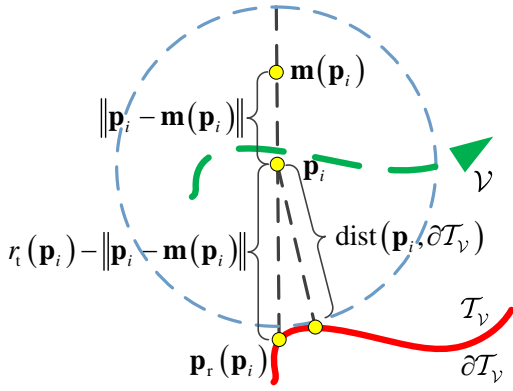


**Figure 12.** The reason for proposing the modified safety radius..

**Proposition 2.** For any  $\mathbf{p}_i \in \mathcal{T}_V$ , if there exists

$$r_t(\mathbf{p}_i) - \|\mathbf{p}_i - \mathbf{m}(\mathbf{p}_i)\| > r'_s, \quad (24)$$

then it is obtained that  $\mathcal{S}_i \subset \mathcal{T}_V$ .

*Proof.* If (24) holds, then  $\mathbf{p}_i \in \mathcal{C}(\mathbf{p}_i) \cap \mathcal{S}_{\mathcal{T}_V}$ , namely  $\mathbf{p}_i \in \mathcal{S}_{\mathcal{T}_V}$ . This implies that  $\text{dist}(\mathbf{p}_i, \partial \mathcal{T}_V) \geq r_s$ , namely  $\mathcal{S}_i \subset \mathcal{T}_V$ .  $\square$

Then, a unified barrier function for the  $i$ th robot keeping within the tube is defined as

$$V_{t,i} = \frac{k_3 \sigma_t(d_{t,i})}{(1 + \epsilon_t) d_{t,i} - r'_s s \left( \frac{d_{t,i}}{r'_s}, \epsilon_s \right)}, \quad (25)$$

where  $\epsilon_t > 0$ . Here, the smooth function  $\sigma(\cdot)$  in (10) is defined as  $\sigma_t(x) \triangleq \sigma(x, r'_s, r_a)$ . The function  $V_{t,i}$  has similar properties to  $V_{m,ij}$ .

- (i)  $\partial V_{t,i} / \partial d_{t,i} \leq 0$  as  $V_{t,i}$  is a nonincreasing function with respect to  $d_{t,i}$ .
- (ii) If  $d_{t,i} > r_a$ , namely  $\mathcal{A}_i \cap \partial \mathcal{T}_V \neq \emptyset$ , then  $V_{t,i} = 0$  and  $\partial V_{t,i} / \partial d_{t,i} = 0$ ; if  $V_{t,i} = 0$ , then  $d_{t,i} > r_a$ .
- (iii) If  $d_{t,i} < r'_s$ , namely  $\mathcal{S}_i \cap \partial \mathcal{T}_V \neq \emptyset$ , then there exists a sufficiently small  $\epsilon_s > 0$  such that

$$V_{t,ij} = \frac{k_2}{\epsilon_t d_{t,i}} \geq \frac{k_2}{\epsilon_t r'_s}.$$

The objective of the designed velocity command is to make  $V_{t,i}$  zero or as small as possible. This implies that  $d_{t,i} > r'_s$ , namely the  $i$ th robot will keep within the tube.

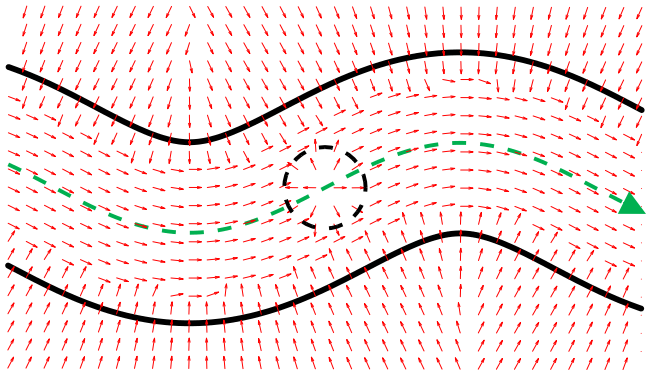


**Figure 13.** Vector field of a curve virtual tube with the modified controller (26).

#### 4.6.3 Modified Swarm Controller with a Non-Potential Term

The modified swarm controller is proposed as

$$\mathbf{v}_{c,i} = \mathbf{v}_{\text{mdf}}(\mathcal{T}_V, \mathbf{p}_i, \mathbf{p}, r'_s), \quad (26)$$

where

$$\begin{aligned} \mathbf{v}_{\text{mdf}}(\mathcal{T}_V, \mathbf{p}_i, \mathbf{p}, r'_s) &\triangleq -\text{sat} \left( \underbrace{-v_{m,i} \mathbf{t}_c(\mathbf{p}_i)}_{\text{Line Approaching}} \right. \\ &\quad \left. + \sum_{j \in \mathcal{N}_{m,i}} \underbrace{-b_{ij} \tilde{\mathbf{p}}_{m,ij}}_{\text{Robot Avoidance}} + \underbrace{(\mathbf{I}_2 - \mathbf{t}_c(\mathbf{p}_i) \mathbf{t}_c^T(\mathbf{p}_i)) \mathbf{c}_i}_{\text{Virtual Tube Keeping}}, v_{m,i} \right). \end{aligned}$$

Here  $(\mathbf{I}_2 - \mathbf{t}_c(\mathbf{p}_i) \mathbf{t}_c^T(\mathbf{p}_i)) \mathbf{c}_i$  is the modified tube keeping term and  $\mathbf{c}_i$  is expressed as

$$\mathbf{c}_i = \frac{\partial V_{t,i}}{\partial d_{t,i}} \left( \frac{\partial r_t(\mathbf{p}_i)}{\partial \mathbf{p}_i} - \frac{(\mathbf{p}_i - \mathbf{m}(\mathbf{p}_i))^T}{\|\mathbf{p}_i - \mathbf{m}(\mathbf{p}_i)\|} \left( \mathbf{I}_2 - \frac{\partial \mathbf{m}(\mathbf{p}_i)}{\partial \mathbf{p}_i} \right) \right)^T.$$

The non-potential term<sup>4</sup>  $(\mathbf{I}_2 - \mathbf{t}_c(\mathbf{p}_i) \mathbf{t}_c^T(\mathbf{p}_i)) \mathbf{c}_i$  is used to imitate the performance of  $\partial V_{\text{tl},i} / \partial \mathbf{p}_i$  and  $\partial V_{\text{tr},i} / \partial \mathbf{p}_i$ .

Consider a scenario that a robot is moving within a curve virtual tube, in the middle of which there exists another robot. Figure 13 shows the vector field of this curve virtual tube with the modified swarm controller (26).

**Remark 4.** The term  $\mathbf{c}_i$  is the gradient of  $V_{t,i}$ , namely  $\mathbf{c}_i = (\partial V_{t,i} / \partial \mathbf{p}_i)^T$ , which is always orthogonal to one of the boundary curve of  $\partial \mathcal{T}_V$ . And  $(\mathbf{I}_2 - \mathbf{t}_c(\mathbf{p}_i) \mathbf{t}_c^T(\mathbf{p}_i)) \mathbf{c}_i$  is a non-potential velocity command component, which is always orthogonal to  $\mathbf{t}_c(\mathbf{p}_i)$ . For avoiding deadlock, directly applying  $\mathbf{c}_i$  in (20) is not feasible. Hence the use of the single panel method is necessary. For all  $\mathbf{p} \in \mathcal{V}$ ,  $l(\mathbf{p}) > l(\mathbf{p}_a^-(\mathbf{p}))$ ,  $l(\mathbf{p}) < l(\mathbf{p}_a^+(\mathbf{p}))$ , if  $|l_r(\mathbf{p}) - l_l(\mathbf{p})|$  and  $|r_r(\mathbf{p}) - r_l(\mathbf{p})|$  are both very large, then the orientation changes of  $\partial V_{\text{tl},i} / \partial \mathbf{p}_i$  and  $\partial V_{\text{tr},i} / \partial \mathbf{p}_i$  inside the tube may be negligibly small. We can choose appropriate values of  $l_r(\mathbf{p})$ ,  $l_l(\mathbf{p})$ ,  $r_r(\mathbf{p})$ ,  $r_l(\mathbf{p})$ , so that the orientations of  $\partial \phi_l(\mathbf{p}_i, \mathbf{p}) / \partial \mathbf{p}_i$  and  $\partial \phi_r(\mathbf{p}_i, \mathbf{p}) / \partial \mathbf{p}_i$  are both approximately orthogonal to  $\mathbf{t}_c(\mathbf{p}_i)$ . Hence  $\partial V_{\text{tl},i} / \partial \mathbf{p}_i$  and  $\partial V_{\text{tr},i} / \partial \mathbf{p}_i$  are also both approximately orthogonal to  $\mathbf{t}_c(\mathbf{p}_i)$ , which explains why  $(\mathbf{I}_2 - \mathbf{t}_c(\mathbf{p}_i) \mathbf{t}_c^T(\mathbf{p}_i)) \mathbf{c}_i$  can imitate  $\partial V_{\text{tl},i} / \partial \mathbf{p}_i$  and  $\partial V_{\text{tr},i} / \partial \mathbf{p}_i$ .

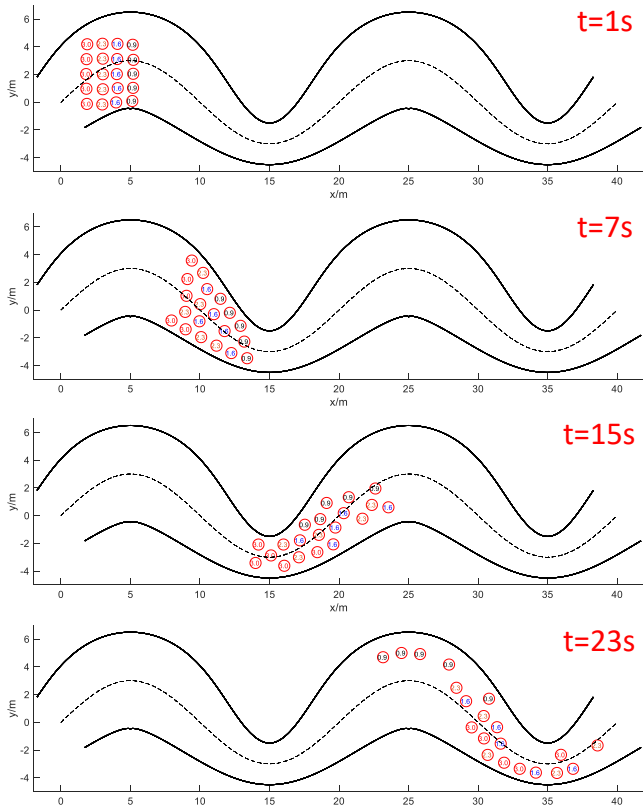


**Figure 14.** Single integral model simulation snapshots.

**Remark 5.** Compared with  $V_{tl,i}$ ,  $V_{tr,i}$  in (17), (18), the unified barrier function  $V_{t,i}$  in (25) has its unique advantage of the broader application. In practice, the case such as  $\text{dist}(\mathbf{p}_i, \partial\mathcal{T}_V) < r_s$  may still happen in practice due to unpredictable uncertainties violating the assumptions. Under this circumstance, the potential functions  $V_{tl,i}$ ,  $V_{tr,i}$  have computation errors, while  $V_{t,i}$  still works well and the modified tube keeping term  $(\mathbf{I}_2 - \mathbf{t}_c(\mathbf{p}_i)\mathbf{t}_c^T(\mathbf{p}_i))\mathbf{c}_i$  dominates the velocity command  $\mathbf{v}_{mdf}(\mathcal{T}_V, \mathbf{p}_i, \mathbf{p}, r'_s)$  in (26), which implies that  $d_{t,i}$  will be increased very fast so that the  $i$ th robot can keep away from the tube boundary immediately.

## 5 Simulation Results

### 5.1 Simulation with the Single Integral Model at Different Maximum Speeds

In this part, the validity and feasibility of the proposed method is numerically verified in a simulation. Consider a scenario that one robotic swarm composed of  $M = 20$  robots passes through a predefined curve virtual tube. All robots satisfy the model in (1). The swarm controller in (26) is applied to guide these robots.

The parameters and initial conditions of the simulation are set as follows. The generating curve is designed manually as a sinusoidal curve in the middle of the curve virtual tube. The width of the tube also changes along the generating curve. The control parameters are  $k_2 = k_3 = 1$ ,  $\epsilon_m = \epsilon_t = \epsilon_s = 10^{-6}$ . All robots with the safety radius  $r_s = 0.4m$ , the avoidance radius  $r_a = 0.8m$  are arranged symmetrically in a rectangular space in the beginning. As shown in Figure 14, the boundaries of the safety area are represented by red circles. To show the ability to control different types of robots

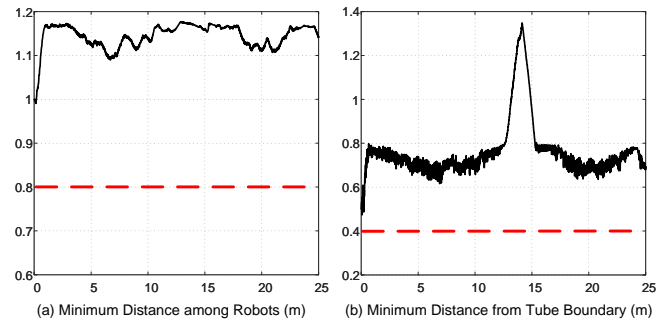


**Figure 15.** Minimum distance among robots and minimum distance from the tube boundary of all robots in the single integral model simulation.

at the same time with our proposed method, the robot's maximum speed is set to four different constants:

$$v_{m,i} = \begin{cases} 3.0\text{m/s} & i = 1, \dots, 5 \\ 2.3\text{m/s} & i = 6, \dots, 10 \\ 1.6\text{m/s} & i = 11, \dots, 15 \\ 0.9\text{m/s} & i = 16, \dots, 20 \end{cases}.$$

The corresponding maximum speed for each robot is shown with different colors in the center of the safety area.

The simulation lasts 25 seconds and three snapshots are shown in Figure 14. It can be observed that the robots at the largest maximum speed  $v_{m,i} = 3.0\text{m/s}$  are in the last column in the beginning. Then they have the trend to overtake other robots ahead. During the whole process, robots can change their relative positions freely instead of maintaining a fixed geometry structure. It is clear from Figure 15(a) that the minimum distance between any two robots is always larger than  $2r_s = 0.8\text{m}$ , which implies that there is no collision among robots. In Figure 15(b), the minimum distance from the tube boundary among all robots keeps larger than  $r_s = 0.4\text{m}$  all the time. Therefore, all robots can avoid collision with each other and keep moving within the curve virtual tube under the proposed swarm controller.

### 5.2 Gazebo-based Simulation with Multicopter Flight Control Rigid Model

In this part, the control performance of the proposed method is specially verified in a multicopter swarm. Different from previous simulations, a multicopter flight control rigid model (Quan 2017, pp. 126-127) is applied to replace the single integral model in (1). In other words, all multicopters are simulated by a six degree of freedom (DOF) nonlinear dynamic model. They are viewed as rigid bodies instead of mass points. A more precise model needs a more detailed and realistic simulation environment. A Gazebo-based simulation environment modified from Tordesillas et al. (2019) is used, which can simulate multiple multicopters at the same time.

As described in (26), the velocity commands for all multicopters are designed by the proposed modified swarm controller. However, the control inputs for the multicopter flight control rigid model are the thrust and moments generated by four propellers. Hence, a inner-loop controller is designed for the multicopter to track the desired velocity. The control parameters are  $k_2 = k_3 = 1$ ,  $\epsilon_m = \epsilon_t = \epsilon_s =$

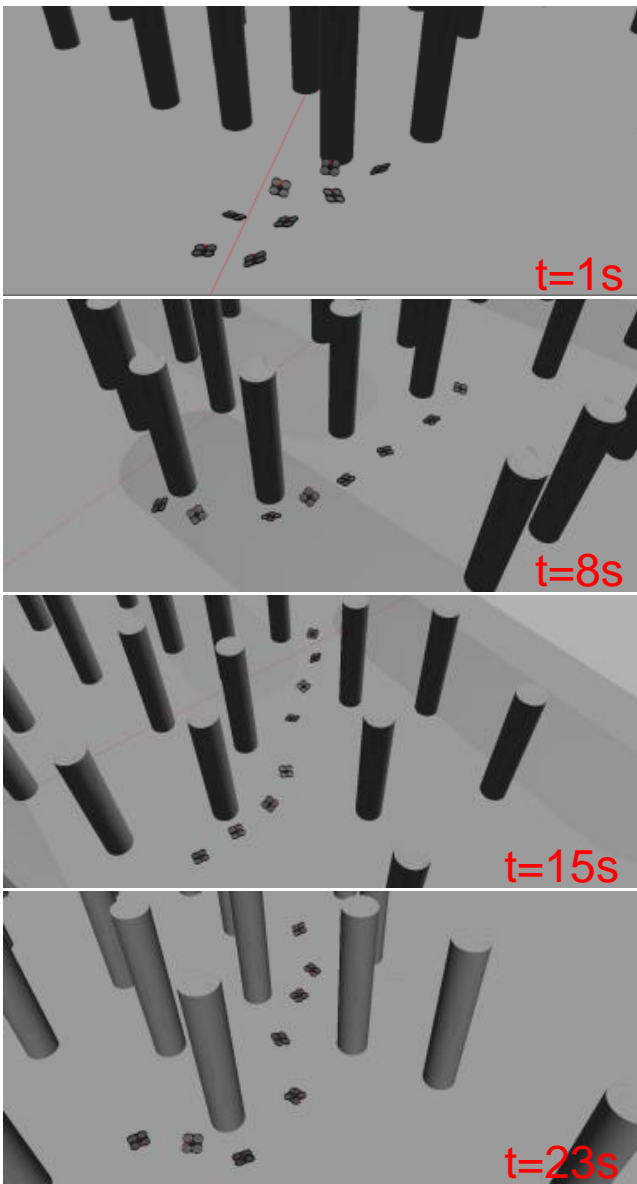


**Figure 16.** Gazebo-based simulation snapshot.

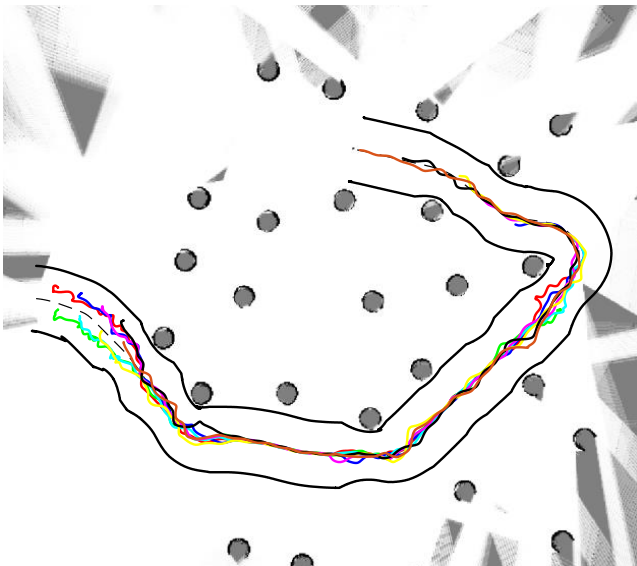


**Figure 17.** Trajectories of the swarm in the Gazebo-based simulation.

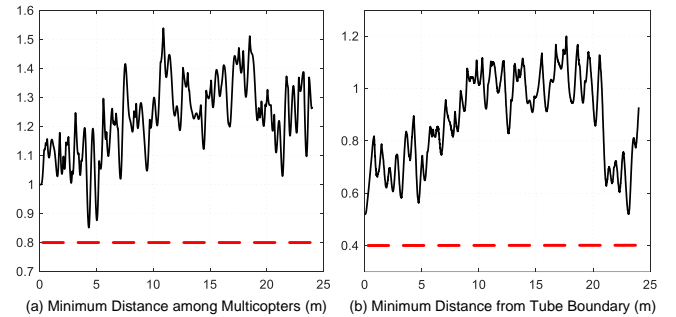


**Figure 18.** Minimum distance among multicopters and minimum distance from the tube boundary of all robots in the Gazebo-based simulation.

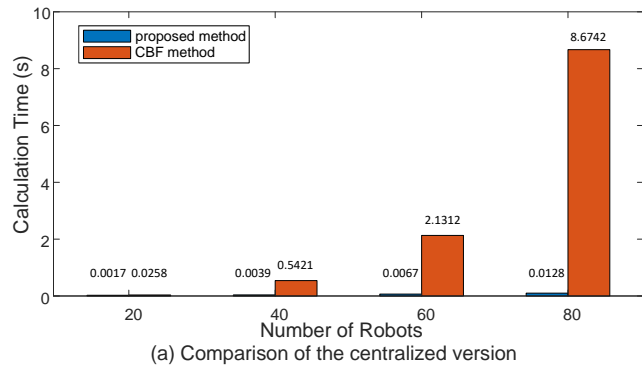
$10^{-6}$ . All robots have the safety radius  $r_s = 0.4\text{m}$ , the avoidance radius  $r_a = 0.8\text{m}$  and the maximum speed  $v_{m,i} = 3\text{m/s}$ .

The simulation is arranged as a “teach-and-repeat” process. To simplify the simulation, all multicopters have the same desired altitude. Given four waypoints  $\mathbf{p}_{wp1} = [20 \ 0]^T\text{m}$ ,  $\mathbf{p}_{wp2} = [32 \ -8]^T\text{m}$ ,  $\mathbf{p}_{wp3} = [41 \ 0]^T\text{m}$ ,  $\mathbf{p}_{wp4} = [31 \ 7]^T\text{m}$ , a first multicopter equipped with a simulated Hokuyo lidar takes off at  $\mathbf{p}_1(0) = [17 \ 0]^T\text{m}$  and then passes all waypoints. The traditional Vector Field Histogram (VHF) method Borenstein et al. (1991) is used to navigate this multicopter and avoid collisions with the obstacles in the environment. In this process, an occupancy map representing the surrounding environment is created from the lidar data. Besides, the flight trajectory is recorded and then utilized to create the curve virtual tube, whose boundary is generated by searching for the closest obstacle in the map. There we have completed the “teach” process.

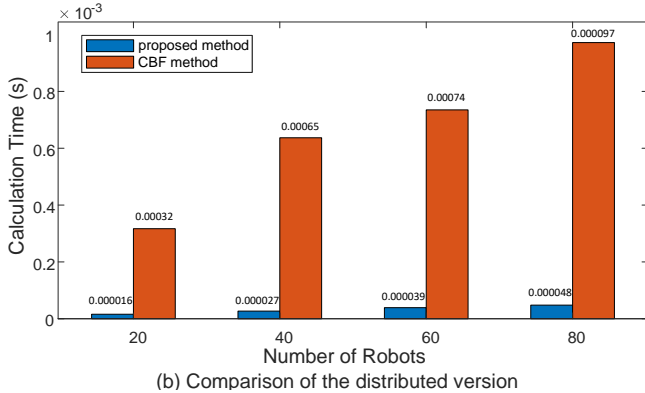
The next is the “repeat” process. We apply  $M = 8$  multicopters composing a multicopter swarm to pass through the curve virtual tube. The initial positions of these eight multicopters are  $\mathbf{p}_2(0) = [18 \ 0.5]^T\text{m}$ ,  $\mathbf{p}_3(0) = [18 \ -0.5]^T\text{m}$ ,  $\mathbf{p}_4(0) = [19 \ 0.2]^T\text{m}$ ,  $\mathbf{p}_5(0) = [19 \ -0.8]^T\text{m}$ ,  $\mathbf{p}_6(0) = [20 \ -0.5]^T\text{m}$ ,  $\mathbf{p}_7(0) = [20 \ -1.5]^T\text{m}$ ,  $\mathbf{p}_8(0) = [21 \ -1]^T\text{m}$ ,  $\mathbf{p}_9(0) = [21 \ -2]^T\text{m}$ . The modified swarm controller (26) is used to guide this swarm. The simulation lasts 23 seconds and four snapshots are shown in Figure 16. The environment map and flight trajectories of these eight multicopters are shown in Figure 17. It is obvious that all multicopters keep flying within the curve virtual tube in the simulation. Similarly to the analysis in the last subsection, as shown in Figure 18(a), the minimum distance between any two multicopters is always larger than  $2r_s = 0.8\text{m}$ , which implies that there is no collision in the swarm. Besides, as shown in Figure 18(b), the minimum distance from the tube boundary among all multicopters keeps larger than  $r_s = 0.4\text{m}$  all the time. Therefore, in this Gazebo-based simulation, all robots successfully avoid colliding with each other and keep flying in the curve virtual tube under the proposed swarm controller.

### 5.3 Comparison of the Calculation Speed With CBF Method

In order to show the advantage of our proposed control method, we compare our method with the CBF method in the



(a) Comparison of the centralized version



(b) Comparison of the distributed version

**Figure 19.** The calculation speed of our proposed method and CBF method.

calculation speed. The controller (26) can be easily converted into a QP controller proposed in Wang et al. (2017). The line approaching term corresponds to the nominal controller. The robot avoidance term and the tube keeping term corresponds to linear inequality constraints. As same as our method, the CBF method also has a distributed version. Here we compare the centralized and distributed versions of these two methods, respectively. The simulation is run on the same computer and record the average calculation time for both methods. Figure 19 shows that our method possesses a much higher calculation speed than the CBF method whether centralized or distributed. For the centralized version, the calculation time of the CBF method will increase rapidly when the number of robots increases, while the calculation time of our method only increases just a little. The reason is that for a dense and complex environment, inequality constraints of the CBF method may become contradictory, which leads to no solution to the QP problem. To deal with this problem, the relaxation variable is an option, but it brings the decline of safety. For the distributed version, the calculation time of both methods are limitedly affected by the increase of robots' number, which strongly expresses the advantage of the distributed methods.

## 6 Experiment Results

A real experiment is carried out in a laboratory room with  $M = 6$  Tello quadcopters and an OptiTrack motion capture system providing the positions and orientations of quadcopters. A laptop computer is connected to Tello quadcopters and OptiTrack with a local wireless network, running the proposed distributed controller (26). The generating curve is designed manually in the middle of

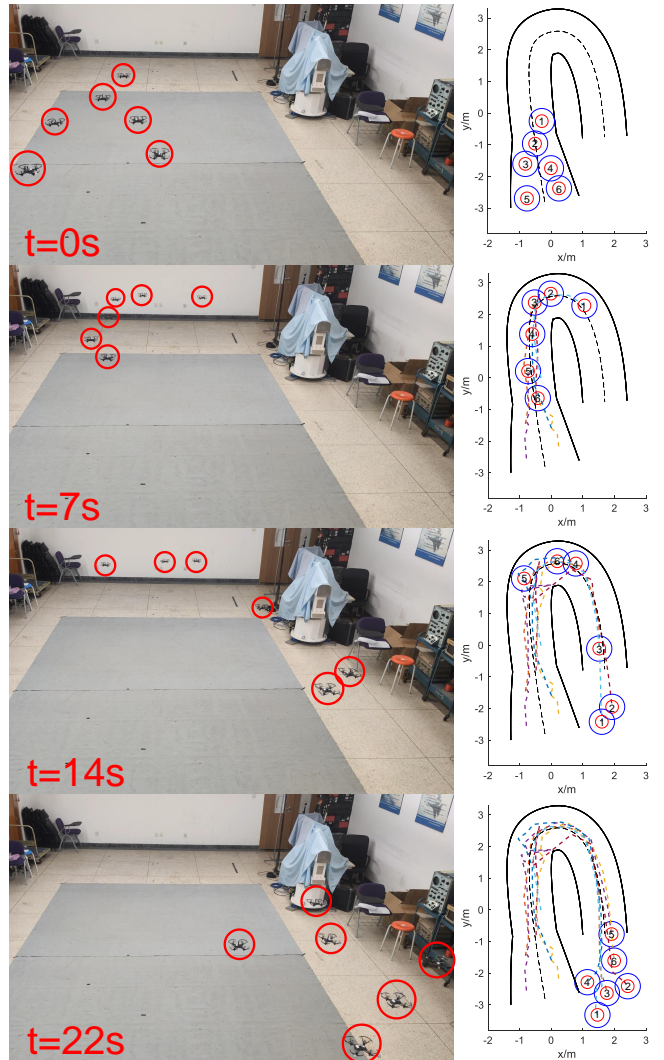


**Figure 20.** Experiment snapshot.

the curve virtual tube, whose width also changes along the generating curve. The control parameters are  $k_2 = k_3 = 1$ ,  $\epsilon_m = \epsilon_t = \epsilon_s = 10^{-6}$ . All quadcopters have the safety radius  $r_s = 0.2m$ , the avoidance radius  $r_a = 0.4m$  and the maximum speed  $v_{m,i} = 0.5m/s$ ,  $i = 1, \dots, 6$ . As shown in Figure 20, the boundaries of the safety and avoidance area are represented by red and blue circles respectively.

The experiment lasts 22 seconds and four snapshots are shown in Figure 20. As same as the numerical simulation, quadcopters can change their relative positions freely instead of maintaining a fixed geometry structure. It can be observed from Figure 21(a) that the minimum distance between any two quadcopters is always larger than  $2r_s = 0.4m$ , which implies that there is no collision among quadcopters. In Figure 21(b), the distances from the tube boundary of all quadcopters keep larger than  $r_s = 0.2m$  when the quadcopters are inside the tube.

## 7 Conclusion

The curve virtual tube passing problem, which includes all robots passing through the tube, inter-robot collision avoidance and keeping within the tube, is proposed and then solved in this paper. Based on the artificial potential

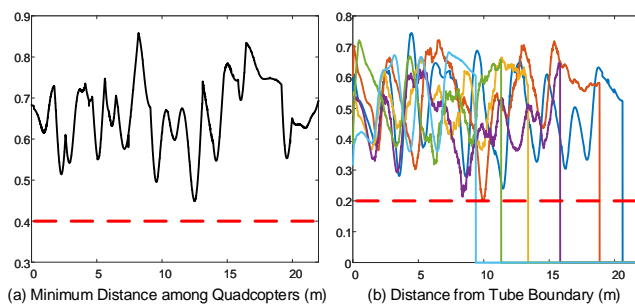


**Figure 21.** Minimum distance among quadcopters and distance from tube boundary. In plot (b), all curves approaching zero means that their corresponding quadcopters have moved across the finishing line of the curve virtual tube, which can be confirmed in the snapshot of  $t = 22$ s in Figure 20.

field method with a control saturation, practical distributed swarm control is proposed for multiple robots to pass through a curve virtual tube. Lyapunov-like functions are designed elaborately, and formal analysis and proofs are made to show that the tube passing problem can be solved, namely all robots avoid collision with each other and keep within the tube in *Lemma 1*, all robots pass through the tube without getting trapped in *Theorem 1*. Simulations and experiments are given to show the effectiveness and performance of the proposed method under different kinds of conditions. To show the advantages of the proposed method over other algorithms in terms of calculation speed of finding feasible solutions, the comparison between our method and CBF method is also presented.

## Notes

1. The points in the same cross section have parallel tangent vectors.
2.  $b_{ij} > 0$  according to the property (i) of  $V_{m,ij}$ .
3. Furthermore, we assume that the  $i$ th robot does not conflict with others except for the  $j_1$ th robot, or not very close to the boundary of the curve virtual tube.
4. The non-potential term refers to a non-conservative vector field with no corresponding scalar potential function. In vector calculus, a non-conservative vector field is a vector field that is not the gradient of any scalar function [Marsden and Tromba \(2003\)](#). A non-conservative vector field is also rotational with its curl non-zero.

## References

Airbus (2019) Airbus skyways: the future of the parcel delivery in smart cities. <https://www.embention.com/project/airbus-parcel-delivery/>.

Antich J and Ortiz A (2005) Extending the potential fields approach to avoid trapping situations. In: *2005 IEEE/RSJ International Conference on Intelligent Robots and Systems*. IEEE, pp. 1386–1391.

Augugliaro F, Schoellig AP and D’Andrea R (2012) Generation of collision-free trajectories for a quadrocopter fleet: A sequential convex programming approach. In: *2012 IEEE/RSJ international conference on Intelligent Robots and Systems*. IEEE, pp. 1917–1922.

Borenstein J, Koren Y et al. (1991) The vector field histogram-fast obstacle avoidance for mobile robots. *IEEE transactions on robotics and automation* 7(3): 278–288.

Chen J, Sun D, Yang J and Chen H (2010) Leader-follower formation control of multiple non-holonomic mobile robots incorporating a receding-horizon scheme. *The International Journal of Robotics Research* 29(6): 727–747.

Chen M, Frazzoli E, Hsu D and Lee WS (2016) Pomdp-lite for robust robot planning under uncertainty. In: *2016 IEEE International Conference on Robotics and Automation (ICRA)*. IEEE, pp. 5427–5433.

Cheung Y, Chung JH and Coleman NP (2009) Semi-autonomous formation control of a single-master multi-slave teleoperation system. In: *2009 IEEE Symposium on Computational Intelligence in Control and Automation*. IEEE, pp. 117–124.

Chung SJ, Paranjape AA, Dames P, Shen S and Kumar V (2018) A survey on aerial swarm robotics. *IEEE Transactions on Robotics* 34(4): 837–855.

Ding W, Gao W, Wang K and Shen S (2019) An efficient b-spline-based kinodynamic replanning framework for quadrotors. *IEEE Transactions on Robotics* 35(6): 1287–1306.

Dolgov D, Thrun S, Montemerlo M and Diebel J (2010) Path planning for autonomous vehicles in unknown semi-structured environments. *The international journal of robotics research* 29(5): 485–501.

Dong X and Sitti M (2020) Controlling two-dimensional collective formation and cooperative behavior of magnetic microrobot swarms. *The International Journal of Robotics Research* 39(5): 617–638.

Gammell JD, Srinivasa SS and Barfoot TD (2014) Informed rrt\*: Optimal sampling-based path planning focused via direct sampling of an admissible ellipsoidal heuristic. In: *2014 IEEE/RSJ International Conference on Intelligent Robots and Systems*. IEEE, pp. 2997–3004.

Gammell JD, Srinivasa SS and Barfoot TD (2015) Batch informed trees (bit\*): Sampling-based optimal planning via the heuristically guided search of implicit random geometric graphs. In: *2015 IEEE international conference on robotics and automation (ICRA)*. IEEE, pp. 3067–3074.

Gao F, Wang L, Wang K, Wu W, Zhou B, Han L and Shen S (2019) Optimal trajectory generation for quadrotor teach-and-repeat. *IEEE Robotics and Automation Letters* 4(2): 1493–1500.

Ge SS and Fua CH (2005) Queues and artificial potential trenches for multirobot formations. *IEEE Transactions on Robotics* 21(4): 646–656.

Hao ND, Mohamed B, Rafaralahy H and Zasadzinski M (2016) Formation of leader-follower quadrotors in cluttered environment. In: *2016 American Control Conference (ACC)*. IEEE, pp. 6477–6482.

Harabor D and Grastien A (2011) Online graph pruning for pathfinding on grid maps. In: *Proceedings of the AAAI Conference on Artificial Intelligence*, volume 25. pp. 1114–1119.

Hernández-Martínez EG and Aranda-Bricaire E (2011) *Convergence and collision avoidance in formation control: A survey of the artificial potential functions approach*. INTECH Open Access Publisher Rijeka, Croatia.

Kavraki LE, Svestka P, Latombe JC and Overmars MH (1996) Probabilistic roadmaps for path planning in high-dimensional configuration spaces. *IEEE transactions on Robotics and*

*Automation* 12(4): 566–580.

Khan MU, Li S, Wang Q and Shao Z (2016) Distributed multirobot formation and tracking control in cluttered environments. *ACM Transactions on Autonomous and Adaptive Systems (TAAS)* 11(2): 1–22.

Khatib O (1986) Real-time obstacle avoidance for manipulators and mobile robots. In: *Autonomous robot vehicles*. Springer, pp. 396–404.

Kim JO and Khosla P (1992) *Real-time obstacle avoidance using harmonic potential functions*. PhD Thesis, Carnegie Mellon University.

LaValle SM and Kuffner Jr JJ (2001) Randomized kinodynamic planning. *The international journal of robotics research* 20(5): 378–400.

Likhachev M, Gordon GJ and Thrun S (2003) Ara\*: Anytime a\* with provable bounds on sub-optimality. *Advances in neural information processing systems* 16: 767–774.

Liu S, Watterson M, Mohta K, Sun K, Bhattacharya S, Taylor CJ and Kumar V (2017) Planning dynamically feasible trajectories for quadrotors using safe flight corridors in 3-d complex environments. *IEEE Robotics and Automation Letters* 2(3): 1688–1695.

Luis CE and Schoellig AP (2019) Trajectory generation for multiagent point-to-point transitions via distributed model predictive control. *IEEE Robotics and Automation Letters* 4(2): 375–382.

Luo Y, Bai H, Hsu D and Lee WS (2019) Importance sampling for online planning under uncertainty. *The International Journal of Robotics Research* 38(2-3): 162–181.

Luo Y, Cai P, Bera A, Hsu D, Lee WS and Manocha D (2018) Porca: Modeling and planning for autonomous driving among many pedestrians. *IEEE Robotics and Automation Letters* 3(4): 3418–3425.

Marsden JE and Tromba A (2003) *Vector calculus*. Macmillan.

Mellinger D, Kushleyev A and Kumar V (2012) Mixed-integer quadratic program trajectory generation for heterogeneous quadrotor teams. In: *2012 IEEE international conference on robotics and automation*. IEEE, pp. 477–483.

Miao Z, Thakur D, Erwin RS, Pierre J, Wang Y and Fierro R (2016) Orthogonal vector field-based control for a multi-robot system circumnavigating a moving target in 3d. In: *2016 IEEE 55th Conference on Decision and Control (CDC)*. IEEE, pp. 6004–6009.

Morgan D, Subramanian GP, Chung SJ and Hadaegh FY (2016) Swarm assignment and trajectory optimization using variable-swarm, distributed auction assignment and sequential convex programming. *The International Journal of Robotics Research* 35(10): 1261–1285.

Oh KK, Park MC and Ahn HS (2015) A survey of multi-agent formation control. *Automatica* 53: 424–440.

Panagou D (2014) Motion planning and collision avoidance using navigation vector fields. In: *2014 IEEE International Conference on Robotics and Automation (ICRA)*. IEEE, pp. 2513–2518.

Panagou D (2016) A distributed feedback motion planning protocol for multiple unicycle agents of different classes. *IEEE Transactions on Automatic Control* 62(3): 1178–1193.

Panagou D, Stipanović DM and Voulgaris PG (2015) Distributed coordination control for multi-robot networks using lyapunov-like barrier functions. *IEEE Transactions on Automatic Control* 61(3): 617–632.

Park J, Kim J, Jang I and Kim HJ (2020) Efficient multi-agent trajectory planning with feasibility guarantee using relative bernstein polynomial. In: *2020 IEEE International Conference on Robotics and Automation (ICRA)*. IEEE, pp. 434–440.

Quan Q (2017) *Introduction to multicopter design and control*. Singapore: Springer.

Quan Q, Fu R and Cai KY (2021a) How far two uavs should be subject to communication uncertainties. *arXiv preprint arXiv:2110.09391*.

Quan Q, Fu R, Li M, Wei D, Gao Y and Cai KY (2021b) Practical distributed control for vtol uavs to pass a virtual tube. *IEEE Transactions on Intelligent Vehicles*.

Rasekhipour Y, Khajepour A, Chen SK and Litkouhi B (2016) A potential field-based model predictive path-planning controller for autonomous road vehicles. *IEEE Transactions on Intelligent Transportation Systems* 18(5): 1255–1267.

Ren W and Sorensen N (2008) Distributed coordination architecture for multi-robot formation control. *Robotics and Autonomous Systems* 56(4): 324–333.

Rezende AM, Gonçalves VM, Nunes AH and Pimenta LC (2020) Robust quadcopter control with artificial vector fields. In: *2020 IEEE International Conference on Robotics and Automation (ICRA)*. IEEE, pp. 6381–6387.

Rimon E (1990) *Exact robot navigation using artificial potential functions*. PhD Thesis, Yale University.

Rostami SMH, Sangaiah AK, Wang J and Liu X (2019) Obstacle avoidance of mobile robots using modified artificial potential field algorithm. *EURASIP Journal on Wireless Communications and Networking* 2019(1): 1–19.

Saska M, Hert D, Baca T, Krátký V and do Nascimento TP (2020) Formation control of unmanned micro aerial vehicles for straitened environments. *Auton. Robots* 44(6): 991–1008.

Slotine JJE, Li W et al. (1991) *Applied nonlinear control*, volume 199. Prentice hall Englewood Cliffs, NJ.

Tahir H, Syed MN and Baroudi U (2019) Heuristic approach for real-time multi-agent trajectory planning under uncertainty. *IEEE Access* 8: 3812–3826.

Tang S, Thomas J and Kumar V (2018) Hold or take optimal plan (hoop): A quadratic programming approach to multi-robot trajectory generation. *The International Journal of Robotics Research* 37(9): 1062–1084.

Thomas GB, Finney RL, Weir MD and Giordano FR (2003) *Thomas' calculus*. Addison-Wesley Reading.

Tony LA, Ratnoo A and Ghose D (2020) Corridorone: Corridors for drones, an adaptive on-demand multi-lane design and testbed. *arXiv preprint arXiv:2012.01019*.

Tordesillas J, Lopez BT and How JP (2019) Faster: Fast and safe trajectory planner for flights in unknown environments. In: *2019 IEEE/RSJ international conference on intelligent robots and systems (IROS)*. IEEE, pp. 1934–1940.

Turpin M, Michael N and Kumar V (2014) Capt: Concurrent assignment and planning of trajectories for multiple robots. *The International Journal of Robotics Research* 33(1): 98–112.

Vadakkepat P, Tan KC and Ming-Liang W (2000) Evolutionary artificial potential fields and their application in real time

robot path planning. In: *Proceedings of the 2000 congress on evolutionary computation. CEC00 (Cat. No. 00TH8512)*, volume 1. IEEE, pp. 256–263.

Wang L, Ames AD and Egerstedt M (2016) Multi-objective compositions for collision-free connectivity maintenance in teams of mobile robots. In: *2016 IEEE 55th Conference on Decision and Control (CDC)*. IEEE, pp. 2659–2664.

Wang L, Ames AD and Egerstedt M (2017) Safety barrier certificates for collisions-free multirobot systems. *IEEE Transactions on Robotics* 33(3): 661–674.

Wolf MT and Burdick JW (2008) Artificial potential functions for highway driving with collision avoidance. In: *2008 IEEE International Conference on Robotics and Automation*. IEEE, pp. 3731–3736.

Xu Y, Zhao S, Luo D and You Y (2020) Affine formation maneuver control of high-order multi-agent systems over directed networks. *Automatica* 118: 109004.

Zhao S and Zelazo D (2019) Bearing rigidity theory and its applications for control and estimation of network systems: Life beyond distance rigidity. *IEEE Control Systems Magazine* 39(2): 66–83.

Zhou X, Zhu J, Zhou H, Xu C and Gao F (2021) Ego-swarm: A fully autonomous and decentralized quadrotor swarm system in cluttered environments. In: *2021 IEEE International Conference on Robotics and Automation (ICRA)*. IEEE, pp. 4101–4107.

## Appendix A. Proof of Lemma 1

Since we have

$$\text{sat}(k_1 l(\mathbf{x}) \eta(\mathbf{x}) \mathbf{t}_c(\mathbf{x}), v_{m,i}) = \kappa_{v_{m,i}} k_1 l(\mathbf{x}) \eta(\mathbf{x}) \mathbf{t}_c(\mathbf{x})$$

where

$$\kappa_{v_{m,i}} = \begin{cases} \frac{1}{k_1 \eta(\mathbf{x}) |l(\mathbf{x})|} & |k_1 l(\mathbf{x}) \eta(\mathbf{x})| \leq v_{m,i} \\ \frac{v_{m,i}}{k_1 \eta(\mathbf{x}) |l(\mathbf{x})|} & |k_1 l(\mathbf{x}) \eta(\mathbf{x})| > v_{m,i} \end{cases}.$$

Then, the function (8) is rewritten as

$$V_{li}(\mathbf{y}) = \int_{\mathcal{V}_y} \kappa_{v_{m,i}} k_1 l(\mathbf{x}) \eta(\mathbf{x}) \mathbf{t}_c(\mathbf{x})^T d\mathbf{x}. \quad (27)$$

With (7), the function (27) becomes

$$\begin{aligned} V_{li}(\mathbf{y}) &= \int_{\mathcal{V}_y} \kappa_{v_{m,i}} k_1 l(\mathbf{x}) d\mathbf{l}(\mathbf{x}) \\ &= \int_{\mathcal{V}_y} \frac{\kappa_{v_{m,i}}}{2k_1} d|k_1 l(\mathbf{x})|^2 \\ &= \int_0^{|k_1 l(\mathbf{y})|} \frac{\kappa_{v_{m,i}}}{2k_1} dz^2 \end{aligned} \quad (28)$$

where  $z = |k_1 l(\mathbf{x})|$ . According to (28), since  $\frac{\kappa_{v_{m,i}}}{2k_1} > 0$ , we have  $V_{li}(\mathbf{y}) > 0$  if  $|l(\mathbf{y})| \neq 0$ , and  $V_{li}(\mathbf{y}) = 0$  if and only if  $|l(\mathbf{y})| = 0$ . When there exists  $|k_1 l(\mathbf{x}) \eta(\mathbf{x})| > v_{m,i}$ , it is obtained that  $\frac{v_{m,i}}{k_1 \eta(\mathbf{x}) |l(\mathbf{x})|} < 1$ . Hence we have  $\kappa_{v_{m,i}} \leq 1$  and

$$\begin{aligned} V_{li}(\mathbf{y}) &\geq \int_0^{|k_1 l(\mathbf{y})|} \frac{1}{2k_1} \frac{v_{m,i}}{k_1 \eta(\mathbf{x}) |l(\mathbf{x})|} dz^2 \\ &\geq \int_0^{|k_1 l(\mathbf{y})|} \frac{v_{m,i}}{2k_1 \eta_{\max}} \frac{1}{z} dz^2 \\ &= \frac{v_{m,i}}{\eta_{\max}} |l(\mathbf{y})|. \end{aligned} \quad (29)$$

If  $\|\mathbf{y}\| \rightarrow \infty$ , then  $\|\mathbf{y} - \mathbf{p}_f\| \rightarrow \infty$ . Since  $\|\mathbf{y} - \mathbf{p}_f\|$  is the shortest distance from  $\mathbf{y}$  to  $\mathbf{p}_f$ , we have  $|l(\mathbf{y})| \geq \|\mathbf{y} - \mathbf{p}_f\|$ . Therefore, from (29), we have  $V_{li}(\mathbf{y}) \rightarrow \infty$ . This also implies that if  $V_{li}(\mathbf{y})$  is bounded, then  $\|\mathbf{y}\|$  is bounded.  $\square$

## Appendix B. Proof of Lemma 2

The reason why these robots are able to avoid conflict with each other will be proved by contradiction. Without loss of generality, assume that  $\|\tilde{\mathbf{p}}_{m,ij_1}(t_2)\| = 2r_s$  occurs at  $t_2 > 0$  first, namely there is a conflict between the  $i$ th robot and the  $j_1$ th robot. Besides, we have  $\|\tilde{\mathbf{p}}_{m,ij}(t_2)\| > 2r_s$  for  $j \neq j_1$ . Consequently,  $V_{m,ij}(t_2) \geq 0$  if  $j \neq j_1$ . Since  $V(0) > 0$  and  $\dot{V}(t) \leq 0$ , the function  $V$  satisfies  $V(t_2) \leq V(0)$ ,  $t \in [0, \infty)$ . By the definition of  $V$ , we have  $V_{m,ij_1}(t_2) \leq V(0)$ . Given any  $\epsilon_{rs} > 0$ , there exists a  $\epsilon_s > 0$ , such that  $s(1, \epsilon_s) = 1 - \epsilon_{rs}$ . Then, at the time  $t_2$ , the denominator of  $V_{m,ij_1}$  defined in (13) is

$$\begin{aligned} &(1 + \epsilon_m) \|\tilde{\mathbf{p}}_{m,ij_1}(t_2)\| - 2r_s s\left(\frac{\|\tilde{\mathbf{p}}_{m,ij_1}(t_2)\|}{2r_s}, \epsilon_s\right) \\ &= 2r_s (1 + \epsilon_m) - 2r_s (1 - \epsilon_{rs}) \\ &= 2r_s (\epsilon_m + \epsilon_{rs}) \end{aligned}$$

where  $\epsilon_{rs} > 0$  can be sufficiently small if  $\epsilon_s$  is sufficiently small. According to the definition in (13), we have

$$\frac{1}{2r_s (\epsilon_m + \epsilon_{rs})} = \frac{V_{m,ij_1}(t_2)}{k_2} \leq \frac{V(0)}{k_2}$$

where  $\sigma_m(\|\tilde{\mathbf{p}}_{m,ij_1}\|) = 1$  is used. Consequently,  $V(0)$  is *unbounded* as  $\epsilon_m \rightarrow 0$  and  $\epsilon_{rs} \rightarrow 0$ . On the other hand, for any  $j$ , we have  $\|\tilde{\mathbf{p}}_{m,ij}(0)\| > 2r_s$  by *Assumption 3*. Let  $\|\tilde{\mathbf{p}}_{m,ij}(0)\| = 2r_s + \epsilon_{m,ij}$ ,  $\epsilon_{m,ij} > 0$ . Then, at the time  $t = 0$ , the denominator of  $V_{m,ij}$  defined in (13) is

$$\begin{aligned} &(1 + \epsilon_m) \|\tilde{\mathbf{p}}_{m,ij}(0)\| - 2r_s s\left(\frac{\|\tilde{\mathbf{p}}_{m,ij}(0)\|}{2r_s}, \epsilon_s\right) \\ &\geq (1 + \epsilon_m) (2r_s + \epsilon_{m,ij}) - 2r_s \bar{s}\left(\frac{\|\tilde{\mathbf{p}}_{m,ij}(0)\|}{2r_s}\right) \\ &= 2r_s \epsilon_m + (1 + \epsilon_m) \epsilon_{m,ij}. \end{aligned}$$

Then we have

$$V_{m,ij}(0) \leq \frac{k_2}{2r_s \epsilon_m + (1 + \epsilon_m) \epsilon_{m,ij}}.$$

Consequently,  $V_{m,ij}(0)$  is still bounded as  $\epsilon_m \rightarrow 0$  no matter what  $\epsilon_{rs}$  is. According to the definition of  $V(0)$ ,  $V(0)$  is still *bounded* as  $\epsilon_m \rightarrow 0$  and  $\epsilon_{rs} \rightarrow 0$ . This is a contradiction. Thus there exists  $\|\tilde{\mathbf{p}}_{m,ij}(t)\| > 2r_s$  for  $i, j = 1, \dots, N, i \neq j, t \in [0, \infty)$ . Therefore, the robot can avoid any other robot by the velocity command (20).

The reason why a robot can stay within the curve virtual tube is similar to the above proof. It can be proved by contradiction as well. Without loss of generality, assume that  $\text{dist}(\mathbf{p}_i(t_3), \partial\mathcal{T}_V) = r_s$  occurs at  $t_3 > 0$ , namely a conflict happens. Similar to the above proof, we can also get a contradiction.  $\square$

## Appendix C. Proof of Theorem 1

According to *Lemma 2*, these robots are able to avoid conflict with each other and keep within the curve virtual tube,

namely  $\mathcal{S}_i(t) \cap \mathcal{S}_j(t) = \emptyset$ ,  $\mathcal{S}_i(t) \cap \partial\mathcal{T}_V = \emptyset$ ,  $t \in [0, \infty)$  for all  $\mathbf{p}_i(0)$ ,  $i, j = 1, \dots, M$  and  $i \neq j$ . In the following, the reason why the  $i$ th robot is able to approach the cross section  $\mathcal{C}(\mathbf{p}_f)$  is given. As the function  $V$  is not a Lyapunov function, the *invariant set theorem* (Slotine et al. 1991, p. 69) is used to do the analysis here.

- (i) Firstly, we will study the property of the function  $V$ . Let  $\Omega = \{\mathbf{p}_1, \dots, \mathbf{p}_M : V \leq l\}$ ,  $l > 0$ . According to *Lemma 2*, there exists  $V_{m,ij}$ ,  $V_{l,i}$ ,  $V_{tr,i} > 0$ . Therefore,  $V \leq l$  implies  $\sum_{i=1}^M V_{l,i} \leq l$ . Furthermore, according to *Lemma 1(iii)*,  $\Omega$  is bounded. When  $\|[\mathbf{p}_1, \dots, \mathbf{p}_M]\| \rightarrow \infty$ , then  $\sum_{i=1}^M V_{l,i} \rightarrow \infty$  according to *Lemma 1(ii)*, namely  $V \rightarrow \infty$ . Therefore the function  $V$  satisfies the condition that the invariant set theorem requires.
- (ii) Secondly, we will find the largest invariant set. It is obtained that  $\dot{V} = 0$  if and only if

$$\begin{aligned} \kappa_{v_{m,i}} k_1 l(\mathbf{p}_i) \eta(\mathbf{p}_i) \mathbf{t}_c(\mathbf{p}_i) - \sum_{j=1, j \neq i}^M b_{ij} \tilde{\mathbf{p}}_{m,ij} \\ + \left( \frac{\partial V_{l,i}}{\partial \mathbf{p}_i} \right)^T + \left( \frac{\partial V_{tr,i}}{\partial \mathbf{p}_i} \right)^T = \mathbf{0}, \end{aligned}$$

where  $i = 1, \dots, M$ . Then we have  $\mathbf{v}_{c,i} = \mathbf{0}$  according to (20). Consequently, the system cannot get “stuck” at an equilibrium point other than  $\mathbf{v}_{c,i} = \mathbf{0}$ .

- (iii) Finally, we will prove that no robot will get “stuck”. Let the 1st robot be ahead of the robotic swarm, namely it is the closest to the finishing line  $\mathcal{C}(\mathbf{p}_f)$ . And the other robots are at back of  $\mathcal{C}(\mathbf{p}_1)$ . When there exists  $\mathbf{v}_{c,1} = \mathbf{0}$ , we examine the following equation related to the 1st robot that

$$\begin{aligned} \kappa_{v_{m,1}} k_1 l(\mathbf{p}_1) \eta(\mathbf{p}_1) \mathbf{t}_c(\mathbf{p}_1) - \sum_{j=2}^M b_{1j} \tilde{\mathbf{p}}_{m,1j} \\ + \left( \frac{\partial V_{l,1}}{\partial \mathbf{p}_1} \right)^T + \left( \frac{\partial V_{tr,1}}{\partial \mathbf{p}_1} \right)^T = \mathbf{0}. \end{aligned} \quad (30)$$

Since the 1st robot is ahead, we have

$$\mathbf{t}_c^T(\mathbf{p}_1) \tilde{\mathbf{p}}_{m,1j} \geq 0 \quad (31)$$

where “=” holds if and only if the  $j$ th robot is as ahead as the 1st one. Then, multiplying the term  $\mathbf{t}_c^T(\mathbf{p}_1)$  at the left side of (30) results in

$$\begin{aligned} \kappa_{v_{m,1}} k_1 l(\mathbf{p}_1) \eta(\mathbf{p}_1) \\ = \mathbf{t}_c^T(\mathbf{p}_1) \sum_{j=2}^M b_{1j} \tilde{\mathbf{p}}_{m,1j} - \mathbf{t}_c^T(\mathbf{p}_1) \left( \frac{\partial V_{l,1}}{\partial \mathbf{p}_1} \right)^T \\ - \mathbf{t}_c^T(\mathbf{p}_1) \left( \frac{\partial V_{tr,1}}{\partial \mathbf{p}_1} \right)^T \geq 0 \end{aligned}$$

where (15), (16), (31) are used. Then we have  $l(\mathbf{p}_1) \geq 0$ . Since  $l(\mathbf{p}_1(0)) < 0$  according to *Assumption 2*, owing to the continuity, given  $\epsilon_0 > 0$ , there must exist a time  $t_{11} > 0$  such that

$$l(\mathbf{p}_1) \geq -\epsilon_0$$

when  $t \geq t_{11}$ . At the time  $t_{11}$ , the 1st robot is removed from the curve virtual tube according to *Assumption 4*. The rest of problem is to consider the  $M - 1$  robots, namely 2nd, 3rd, ...,  $M$ th robots. We can repeat the analysis above to conclude this proof.  $\square$